Jatco

# JATCO TECHNICAL REVIEW

No.25

# CONTENTS

## Preface



## Technical Reports

### Special Feature: Electric Powertrain “X-in-1”

## Product Introduction



## Patent

# A year of “sprout,” an endeavor for the future

Tomoyoshi SATO

President and CEO

The year 2025 is a year of “sprout” for JATCO.

We are excited to begin this year with a new organizational structure via the merger with JATCO Engineering Ltd. More than ever, we are committed to expanding our business by fostering the sprouting of seeds for future growth and establishing a firm business foundation. The term “sprout” here refers not just to a beginning, but a sign of strong growth for the future. Our company has reached its 55th anniversary, and we are accelerating our efforts to pioneer the next era of mobility by using as our groundwork the trust and technology we have accumulated over the years.

Symbolic of this “sprout” is the electrification initiative, which in this year is positioned as the “dawn of e-Axle.” The e-Axle is an important factor in the future of mobility because it is at the core of electrification technology. We will bring a 3-in-1 EV powertrain and a 5-in-1 e-POWER electric unit to the market, aiming to greatly enhance the efficiency and performance of electric vehicles. As a new challenge, we are also developing an ultracompact e-Axle technology that can achieve a higher power density. These are solid steps toward our dream of “installing a JATCO drive unit on every wheel.”

## Symbol of “sprout”: diverse endeavors

The e-Axle is not the only symbol of JATCO’s “sprout,” as the company is sprouting a series of new businesses that extend beyond the framework of mobility in an attempt to contribute to the sustainability of society as a whole.

First, we plan to launch “Lifmy”, a wheelchair with a transfer mechanism, in Japan in early 2026. In an aging society, freedom of movement largely affects quality of life. Within this context, it is important that the Lifmy is more than just a wheelchair: it is also equipped

with innovative mechanisms that support user independence. When presented for the first time at the International Home Care and Rehabilitation Exhibition held at Tokyo Big Sight, it was highly acclaimed by many visitors. This symbolic initiative demonstrates that JATCO uses technology to solve social issues through its sincere commitment to "human mobility."

We further plan to shortly launch a two-speed automatic-transmission in-wheel-motor drive unit for electric motorcycles on the Chinese market. Despite the drive unit having a very simple shifting mechanism, it also has a highly efficient drive performance, enabling the bike to easily tackle steep terrain in, for example, Chinese mountain ranges or make a powerful start even when carrying heavy loads. The new system will therefore serve to expand the "freedom of movement in daily life" as well as the "joy of driving a motorcycle." In the future, we, along with the Chinese OEMs, will aim to expand sales into markets outside of China.

In addition, a model equipped with a GA30, a 2-in-1 drive unit for electric-assist bicycles, will be available in Japan in spring 2026. This product offers a new mobility experience for urban areas and tourist destinations, being both nimble and comfortable to operate and contributing to reducing the company's environmental impact. By bringing new merits to bicycles as a familiar means of transportation, JATCO's technology hopes to redefine the "joy of transportation."

Furthermore, the area of renewable energy is another "sprout area" for our company. The launch of our power generation increaser for medium-sized onshore wind turbines configures a new initiative to extend the reach of our company beyond mobility. Securing the widespread use of clean energy is essential to achieving a sustainable society, to which JATCO will contribute by improving the efficiency of wind power generation through applying the drive and control technologies we have for long developed. This project serves as a testament to the fact that our vision is expanding beyond "mobility" and including "energy," both of which are at the very foundations of our society.

## Vision for the future: "a JATCO on every wheel"

Our dream is to have "a JATCO drive unit on every wheel." This is not just a product strategy but also a vision to expand the possibilities of mobility. In addition to automobiles, JATCO's technological products have created new benefits in diverse areas, including bicycles, wheelchairs, industrial machinery, and renewable energy.

Behind this vision are the challenges faced by society, which encompass achieving carbon neutrality, improving urban transportation efficiency, supporting the aging population, and

providing a stable energy supply. JATCO will continue to be a company that solves these issues through “technology.” The creation of new benefits through electrification, software, and AI use relates not merely to product development efforts but also to a genuine attempt at contributing to the sustainability of society as a whole.

## Message to engineers: nurture the buds, create the forest

The year 2025 is the year to ensure that the sprouted buds will be nurtured to grow into strong trunks, such that the efforts of each engineer will shape JATCO’s future. It takes time and effort to nurture buds, but the day will surely come when these buds will eventually become forests and support the lives of many people worldwide.

We bear the responsibility of paving the way for the next era of mobility while carrying 55 years of company history. JATCO will continue challenging itself to accelerate its global expansion and deliver sustainable mobility. Together, let us keep moving toward our dream of expanding the possibilities of mobility.

# e-Axle for 100% Electric Motor-Driven Hybrid and New Electric Vehicles

Atsumi WATANABE* Susumu YOSHIDA* Naoki KOBAYASHI** Keisuke SUZUKI**

Abstract

This paper describes a new e-Axle developed for 100% electric motor-driven hybrid and new electric vehicles. The e-Axle is JATCO's first unit, which was developed in collaboration with Nissan Motor Co., Ltd. It integrates a motor, inverter, and gearbox to achieve high performance with a compact size and low cost.

## 1. Introduction

In recent years, automobile electrification has rapidly progressed against the backdrop of global warming countermeasures and the need to reduce automobile emissions.

In battery electric vehicles (BEVs) and 100% electric motor-driven hybrid e-POWER-equipped vehicles, reducing aerodynamic drag, increasing battery space, and ensuring collision safety are important issues. To address these at a high level, the size of the drive unit must be reduced. In addition, to deliver the "motor-driven driving performance," which is unique to electric vehicles, new technologies are required to accomplish the aforementioned compactness and high-torque/high-output performance.

This paper describes the new e-Axle, which was developed jointly with Nissan Motor Co., Ltd. for new BEVs and e-POWER-equipped vehicles.

## 2. Objectives of the new e-Axle

To satisfy the high-performance requirements of new BEVs and e-POWER-equipped vehicles, a new e-Axle was developed with the following objectives:

- To reduce the cost by downsizing the unit and the number of parts, which contributes to improved vehicle platform performance
- To improve quietness, which is an attractive feature of electric vehicles
- To improve efficiency for increased driving range
- To share the use of the e-Axle unit in BEVs and e-POWER-equipped vehicles

In developing JATCO's first e-Axle, the unit system was designed to meet these objectives. [1]

*Project Management Department **Powertrain and EV Electrical Technology Department, Nissan Motor Co., Ltd.

## 3. Configuration of the e-Axle unit

The configuration of the e-Axle unit is described separately for BEVs and e-POWER-equipped vehicles as follows:

### 3.1 e-Axle for BEVs

The e-Axle for BEVs has a 3-in-1 configuration that integrates a motor, inverter, and gearbox to reduce size and cost (Fig. 1).

Image Source: Nissan Motor Co. Ltd.

Fig. 1 e-Axle for BEV

### 3.2 e-Axle for e-POWER-equipped vehicles

The e-Axle for e-POWER-equipped vehicles shares as many components as possible with the 3-in-1 e-Axle for BEVs and has a 5-in-1 configuration with an additional generator and a speed increaser (Fig. 2). However, the increase in speed was designed to be smaller than that of the conventional type, and the three-axis configuration was modified into a two-axis configuration.

Image Source: Nissan Motor Co. Ltd.

Fig. 2 e-Axle for e-POWER

## 4. Design goals

### 4.1 Improved quietness

In the new e-Axle, we aimed to reduce high-frequency airborne noise generated by the excitation forces of the motor, inverter, generator, and gearbox. To address this, the housing structure was designed to integrate the components of the motor, inverter, generator, and gearbox. The vibratory force was suppressed by improving the joint rigidity of the housing components and by optimizing the bearing arrangement (Fig. 3).

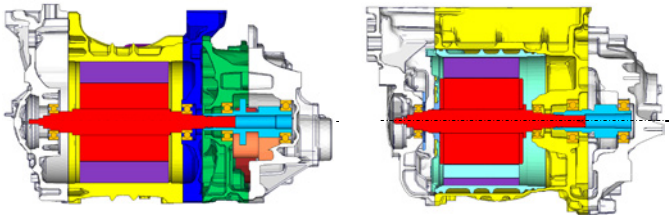

Previous model e-Axle New e-Axle

Fig. 3 e-Axle unit section of BEV [2]

Furthermore, a six-part skew design was used for the rotor core to suppress the higher-order motor vibratory force, which resulted in a significant reduction in solid-state propagation noise. [2]

### 4.2 Improvement of gearbox efficiency

Improving the fuel efficiency of the vehicles equipped with an e-POWER gearbox necessitates an increase in gearbox efficiency. Therefore, losses due to the agitation resistance of the lubricating oil and friction at the gear tooth contact area were reduced.

#### 4.2.1 Reduction of churning loss

A dual-shaft gear set was placed above the unit to reduce the agitation resistance of the lubricating oil. A three-dimensional (3D) simulation of the lubricant flow was performed to simultaneously reduce agitation resistance and gear lubrication.

#### 4.2.2 Reduction of gear meshing loss

The gear tooth contact geometry was optimized via simulations to reduce gear loss.

Altogether, the gearbox loss was reduced by approximately 10% compared to that of the previous e-Axle (Fig. 4).

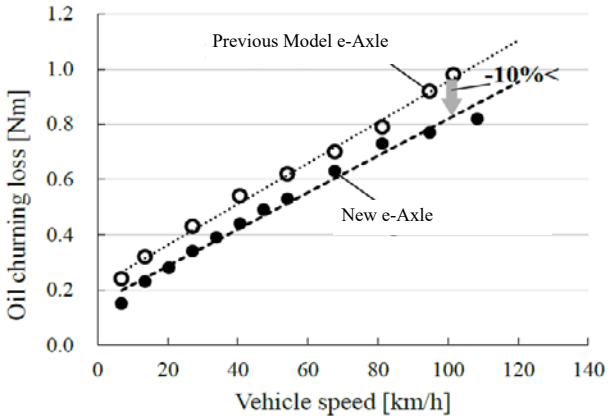


Fig. 4 Gear-box loss [1]

### 4.3 Initiatives for cost reduction

#### 4.3.1 Cost reduction of magnets

The amount of heavy rare-earth metals used in rotor magnets, which account for a large proportion of motor costs, was reduced [1] (Fig. 5).

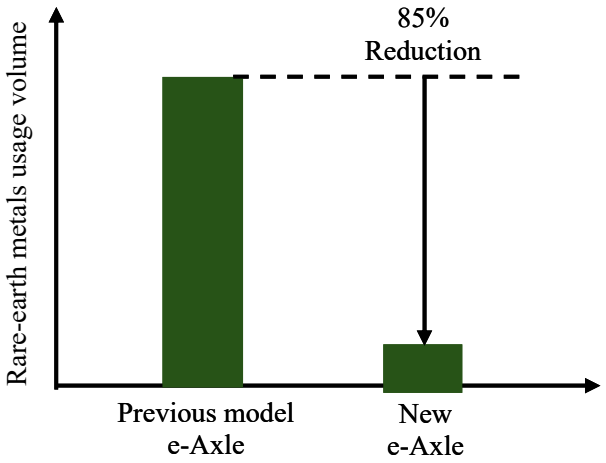


Fig. 5 Rare-earth metal usage volume

#### 4.3.2 Shared use of parts

The e-POWER is a system that appeals to motor-driven driving performance, with a drive mechanism that can be made more compatible with BEVs. Exploiting this feature, an e-Axle that shared the same drive motor and gearbox was designed for BEVs and e-POWER-equipped vehicles, resulting in cost reduction and productivity improvement (Fig. 6).

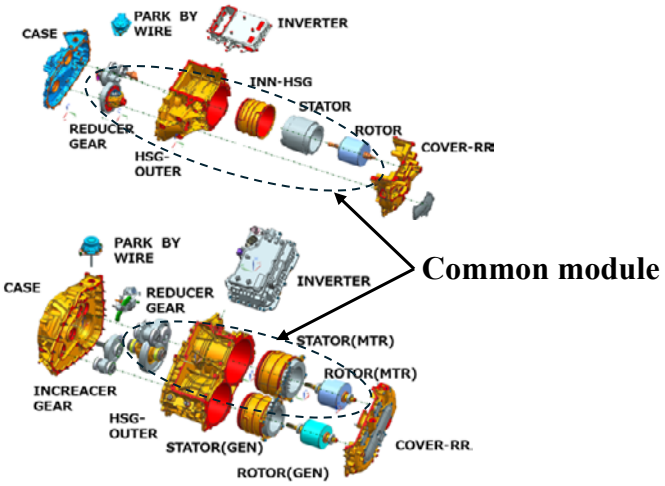


Fig. 6 Module structure concept

## 5. Summary

A new e-Axle was developed for new BEVs and 100% electric motor-driven hybrid vehicles.

- Quietness, an attractive feature of electric vehicles, was improved by increasing the rigidity of the housing structure and introducing a skewed rotor core.
- The design aimed to reduce lubricant agitation resistance and gear friction loss, improving driving range and fuel economy. Gearbox loss was reduced by approximately 10% compared with that of the conventional type.
- Reducing the use of heavy rare-earth metals and sharing their components led to lower cost and higher productivity while meeting the requirements of both BEVs and e-Axle for vehicles equipped with e-POWER.

## 6. References

(1) Sho Maruyama, et al.: Development of EV Powertrain for Third-Generation New EV, Proceedings of the 2025 JSAE Annual Congress (Autumn), 20256148

(2) Kazuhiko Arai, et al.: Development of Integrated 3-in-1 Electric Powertrain and Optimization for Dedicated EV Platform to Improve Powertrain NV, Proceedings of the 2025 JSAE Annual Congress (Autumn), 20256187

■ Authors ■

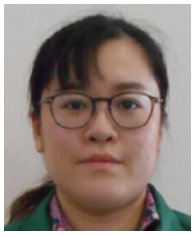
Atsumi WATANABE


Susumu YOSHIDA

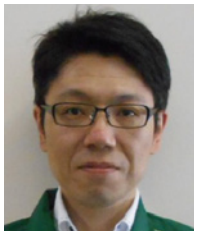
Naoki KOBAYASHI


Keisuke SUZUKI

# Compact High-Torque Motors for e-Axle on New Electric Vehicles

Yu SEKINE* Yusuke TACHIBANA* Atsushi MAEDA* Masatsugu ENDO*
Kohei MUROTA** Koichiro OZAKI**

## Abstract

A new compact high-torque motor was developed for an e-Axle that integrates a motor, an inverter, and a gearbox. To achieve compactness and high torque in the new motor, a thin rectangular-wire was used for the stator coil, and the winding structure was optimized. In this paper, we report on the electromagnetic design and provide an overview of the issues involved in improving productivity.

## 1. Introduction

Recently, automobile electrification has progressed in response to global warming countermeasures and stricter environmental regulations. To meet the requirements of increased cabin space, reduced aerodynamic drag, sufficient space for a battery, and crash safety, the drive unit (e-Axle) integrating a motor, inverter, and gearbox must be downsized. To downsize e-Axle (Fig. 1), it is necessary to reduce the motor size, which accounts for a large proportion of the e-Axle volume and has a significant impact on the unit shape.

To downsize a motor while ensuring sufficient torque and power output, it is important to have a large number of turns in the stator coil (hereinafter referred to as "turn number") within a limited space and to devise a structure that can carry a large current.

A new motor was designed to improve torque per motor volume (hereinafter referred to as "torque density") and power per motor volume (hereinafter referred to as "power density"), which are indicators of compactness and high performance.

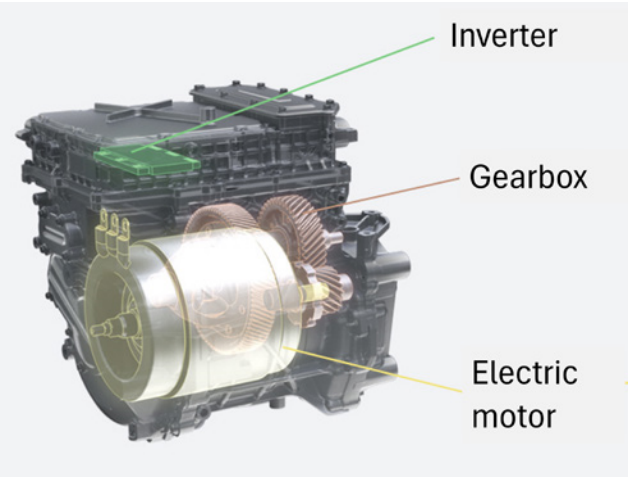


Fig. 1 Main components of e-Axle
Image Source: Nissan Motor Co., Ltd.

*Hardware System Development Department ** Powertrain and EV Electrical Technology Department, Nissan Motor Co., Ltd.

## 2. Winding structure of the stator coil

To achieve miniaturization and high performance, it is important to develop a winding structure for stator coils. The motor for the new e-Axle has a stator coil with a rectangular cross-section made of a rectangular wire (Fig. 2). This structure increases the torque by increasing the number of turns and ensures sufficient power output by optimizing the parallel winding structure.

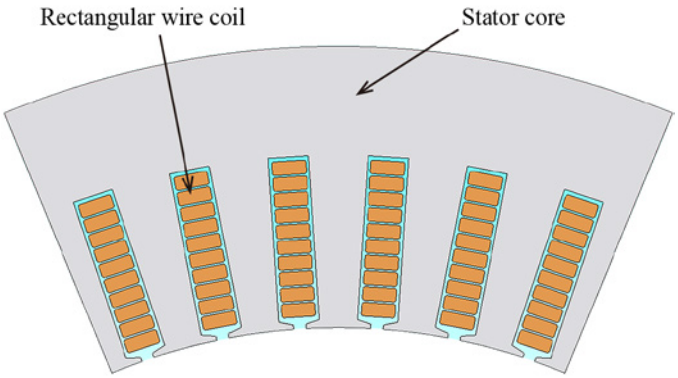


Fig. 2 Stator cross-section

### 2.1 Winding structure for increased motor torque

The torque of an interior permanent magnet synchronous motor (IPMSM) is expressed as follows:

$$T = T_m + T_r = \frac{p}{2}\{\psi_a i_q + (L_d - L_q) i_d i_q\} \quad (1)$$

where $T$ is the motor torque, $T_m$ is the magnetic torque, $T_r$ is the reluctance torque, $P$ is the number of poles, $\psi_a$ is the flux linkage produced by the magnet, $i_d$, $i_q$ are the d- and q-axis currents, respectively, and $L_d$, $L_q$ are the d- and q-axis inductances, respectively.

In general, the contribution of the magnetic torque $T_m$ is high in the high-torque range. Hence, to intuitively show the effect of the winding structure on torque, the magnet torque $T_m = \frac{p}{2}\psi_a i_q$ in equation (1) was studied. The parameters that correlate with the magnetic torque are expressed in Equation (2).

$$T_m \propto \frac{p}{2} N_{turn} N_{series} \Phi I_{coil} \quad (2)$$

where $N_{turn}$ is the turn number per slot, $N_{series}$ is the number of coils in series, $\Phi$ is the magnetic flux, and $I_{coil}$ is the coil current.

The motor torque is proportional to the number of poles, turns, and coils in series, as well as to the magnetic flux and coil current. However, increasing the number of poles and the magnetic flux without changing the motor size has a large cost impact, for instance because of an increase in the number of magnets. In addition, increasing the coil current is difficult because of the limitations of high-power systems such as inverters and the limitations of motor-cooling performance. Therefore, our objective was to increase the magnetic torque by increasing the number of turns.

To increase this number without changing the slot cross-sectional area, it is necessary to reduce the cross-sectional area and clearance of the coil. To reduce the coil cross-sectional area while reducing the coil loss, a thin rectangular-wire was used. In the new e-Axle motor, a competitive 10-turn stator coil was achieved by developing a stator production technology that leverages a thin rectangular-wire.

### 2.2 Winding structure to secure motor power output

The motor output is expressed in Equation (3).

$$P_{out} = \eta P_{in} = \eta 3 V_{phase} I_{phase} cos\theta \quad (3)$$

where $P_{out}$ is the motor power, $\eta$ is the motor efficiency, $P_{in}$ is the motor input power, $V_{phase}$ is the motor phase voltage, $I_{phase}$ is the motor phase current, and $cos\theta$ is the power factor.

In a parallel-winding structure, the input current is distributed across multiple coils; thus, the relationship between the motor phase current and the coil current when the number of coils in parallel is denoted as $N_{parallel}$ is expressed in Equation (4).

$$I_{phase} = N_{\text{parallel}}\, I_{coil} \tag{4}$$

As shown in Figs. 3 (a) and (b), the number of coils per phase is 8, which is the product of the numbers of coils in series and in parallel.

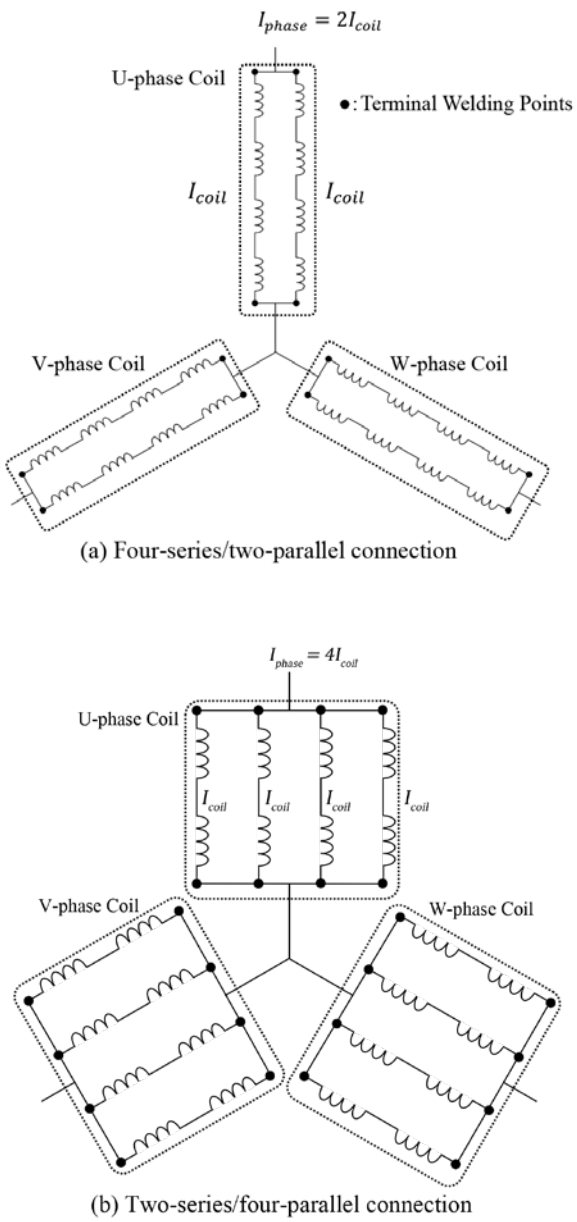


Fig. 3 Three-phase coil connection diagram

To ensure high motor power output, the motor phase current must be proportional to the motor phase voltage, as expressed in Equation (3). However, as expressed in Equation (4), the motor phase current is determined by the product of the coil current and the number of coils in parallel, and the coil current is restricted by the heat resistance and cooling functions. Therefore, a high motor phase current was achieved by increasing the number of coils in parallel.

In the new e-Axle motor, high motor power output is produced using four coils in parallel by improving the welding of the stator and busbar terminals of the rectangular wire.

Competitive torque and power density values were obtained by increasing the number of turns to 10 and the number of coils in parallel to four without increasing the motor size, achieving both high torque and high power output (Fig. 4).

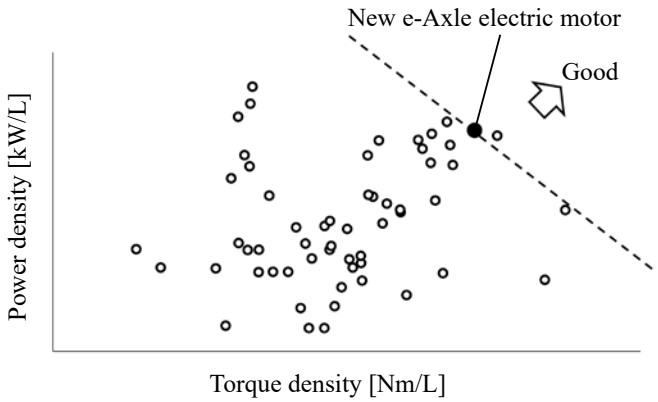


Fig. 4 Torque density vs power density of e-Axle electric motor

## 3. Challenges in ensuring productivity

### 3.1 Formation of thin rectangular-wire coils

Because of the concentration of bending stress during the formation of thin rectangular-wire coils, problems occur when the enamel coating breaks or peels on the tensile side, wrinkles form on the compressive side, and shape variations occur after formation. To ensure that the stress generated in the enameled coating does not exceed the proof stress even after considering variations, the bending dimensions during coil formation were controlled, and the appropriate enameled coating material was selected.

### 3.2 Control of the amount of varnish in the slot

Owing to the use of a 10-turn stator coil with a thin rectangular-wire, the degree of non-uniformity in the clearance within the slot increases. This highlights the need to control the amount of varnish used.

Productivity was ensured by optimizing the injection volume of the varnish such that it could be filled in the shortest amount of time without overflowing, while considering the amount of varnish to guarantee sufficient adherence strength.

### 3.3 Increase in the number of welding strikes

The stator coil and three-phase terminal block busbars were welded together with their respective copper terminals (Fig. 5).

The four-parallel configuration of the rectangular wire resulted in a total of 24 welding points, as indicated by ● in Fig. 3 (b). In response to the increase in the number of welding points, a new and efficient welding method was developed by controlling the positioning and dimensional accuracy in the welding process.

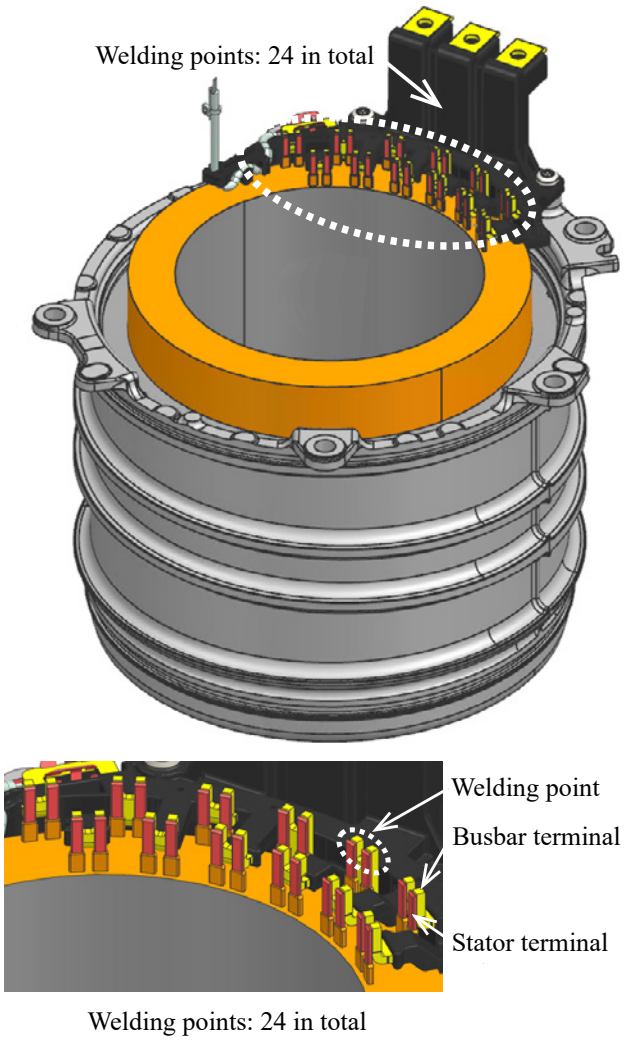


Fig. 5 Welding points of stator coil and busbar

## 4. Summary

- A new type of motor for e-Axle was developed to achieve small size, high torque, and high power output.
- A high torque density was obtained using a thin rectangular-wire for the stator coil, which enabled a high turn number of 10 without increasing the size.
- High power density was achieved by securing sufficient phase currents using four stator coils in parallel.
- To improve productivity, a coil-forming design, control of the amount of varnish in the slot, and welding methods for rectangular wires and busbars were developed.
- Competitive torque and power density values were obtained, making the new e-Axle compact and high-performance.

## 5. Acknowledgements

We express our sincere appreciation to Astemo, Ltd. for their assistance with motor development.

■ Authors ■


Yu SEKINE


Yusuke TACHIBANA


Atsushi MAEDA


Masatsugu ENDO


Kohei MUROTA


Koichiro OZAKI

# Development of X-in-1 TIG Welding Equipment for High-Quality and High-Productivity Welding

Daisuke HITOKOTO* Kouki OKUI* Wenqiang HE*

## Abstract

This report describes the development of a tungsten inert gas (TIG) welding system suitable for joining busbar and stator terminals of the new electric drive unit "X-in-1." TIG welding is used because of its superior welding quality and cost performance compared to conventional laser welding. The report describes how the welding system successfully enabled mass-production by achieving both welding quality and productivity. This was achieved by using a simultaneous clamping jig and a position correction system with a three-dimensional (3D) camera to address the variation issues in the position of busbar terminals and stator terminals as well as in the quality and productivity issues associated with welding at 24 locations.

## 1. Introduction

X-in-1 is a new type of electric drive unit that integrates a motor, a generator, an inverter, and a variable-speed gear within a compact package. The stator coils of the motor and generator are made of flat copper wire (hereinafter referred to as "flat wire") instead of conventional round copper wire. The current is controlled by the inverter and is supplied to the stator coils of the motor and generator through the busbars. The contacts between the busbars and the coils are welded together using copper terminals.

The busbars used in X-in-1 are rigidly molded with resin to guarantee insulation in a compact layout and to ensure durability against driving vibration. The busbars are bolted to the housing near the output terminal of the stator so that the welding terminal is firmly fixed in place.

However, stator terminals, which are the paired welded part, are made with copper wire bent into a three-dimensional (3D) form. This makes it difficult to maintain the position of tip of the welded parts with high precision.

In order to accurately weld a small area of approximately 3 mm square, a new welding equipment was developed by aligning busbar terminals, which are fixed to a rigid body, with stator terminals that are prone to elastic deformation.

This report describes the development of a tungsten inert gas (TIG) welding system that addresses this issue and achieves high target values both in terms of weld quality and productivity.

*Machining Process Engineering Section No.2

## 2. Themes and issues

The overall view of the X-in-1 busbar and stator prior to welding is shown in Fig. 1a). A magnified view of the terminals at the welding point is shown in Fig. 1b).

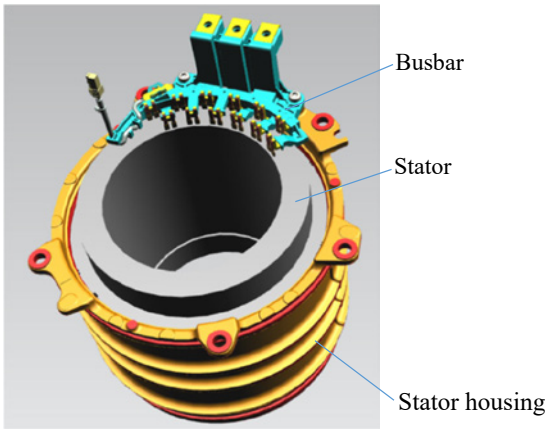


a) X-in-1 stator assembly

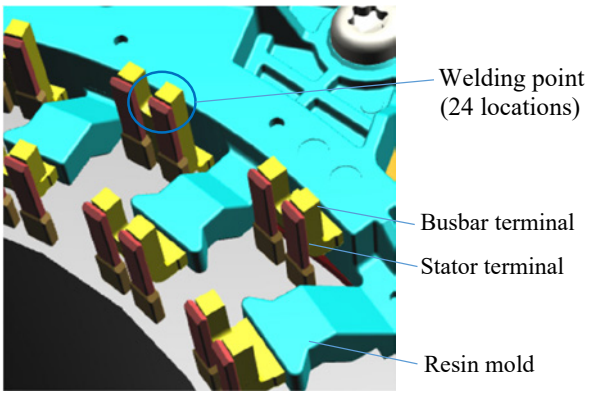


b) Welding terminal

Fig. 1 CAD drawing of X-in-1 stator

There are two welding methods for motor flat wire, namely conventional laser welding and TIG welding. Laser welding is commonly used in Europe and the United States, whilst TIG welding is common in Japan. TIG welding has an advantage in terms of quality and cost, but laser welding has an advantage in terms of welding speed. (Table 1)

Table 1 Comparison of welding methods

| | Laser welding | TIG welding |
|---|---|---|
| Quality (Q) | × Spatter is generated | ○ No spatter |
| Cost (C) | × Welding machines are expensive | ○ Welding machines are inexpensive |
| Time (T) | ○ High welding speed | × Slow welding speed |

Laser welding uses a high-energy laser beam to melt the base metal to weld, but sudden changes in temperature tend to cause violent convection and vaporization of the molten metal, resulting in the risk of spatter. In the case of TIG welding, as shown in Fig. 2, the entire welding point is heated by an umbrella-shaped arc from the tip of the tungsten electrode, which causes gradual liquefaction of the molten part and suppresses spatter generation.

Considering the importance of welding quality, this study used TIG welding to develop a busbar welding method because it eliminates the concern about spatter generation.

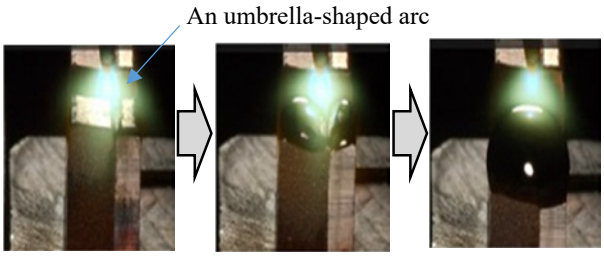


Fig. 2 Progression of TIG welding

## 3. Specification issues of X-in-1 TIG welding equipment

This section explains the three issues that need to be addressed in the development of X-in-1 TIG welding equipment.

### 3.1 TIG welding speed issues

When flat wires are joined using the conventional TIG welding method, the welding operation takes several times longer than using laser welding because the welding machine has to move at each welding point. Fig. 3 illustrates the movement of the welding machine.

[1] Clamp: A terminal clamp that is integrated with the torch grips the terminal to be welded and positions it while maintaining close contact with it.

[2] Touch: The welding torch makes contact with the weld and then moves up to the height at which the arc can be generated. Although the welding terminals have height variations, this movement ensures that the electrode is always at the optimum height.

[3] Weld: The electrode (welding torch) at the appropriate height carries out welding.

[4] Move: After welding, the torch and clamp move to the next weld point, releasing their grip on the terminal and avoiding the already-welded area.

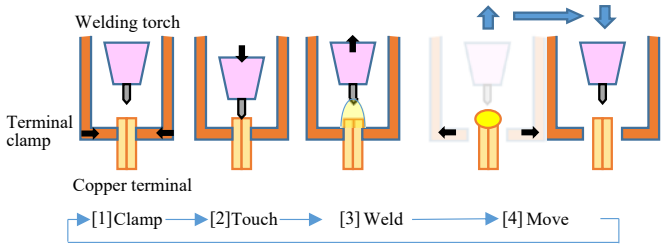


Fig. 3 Conventional TIG welding process

### 3.2 Geometry issues specific to X-in-1 components

As mentioned above, X-in-1 was designed such that the busbar components can carry electric current while set in a compact layout. As a result, the following issues related to mass production became apparent.

[1] There are 24 welding locations, which is about four times as many as other companies' components. Therefore, the production time was prolonged and the risk of weld defects increased.

[2] The busbar is molded with a resin and bolted to the housing, making it rigid.

[3] Because the stator coil terminals are made by 3D bending of copper wire, the positional precision of the terminal tip varies greatly, and misalignment with fixed busbar terminals is likely to occur.

[4] The X-in-1 motor and generator have different stator specifications for a total of five models, resulting in setup losses.

### 3.3 Weld quality issues

There are two main quality requirements post TIG welding. They are:

[1] To ensure that the welded parts have sufficient tensile breaking strength

[2] To prevent blistering on the enameled part of the flat-wire insulation (Fig. 4).

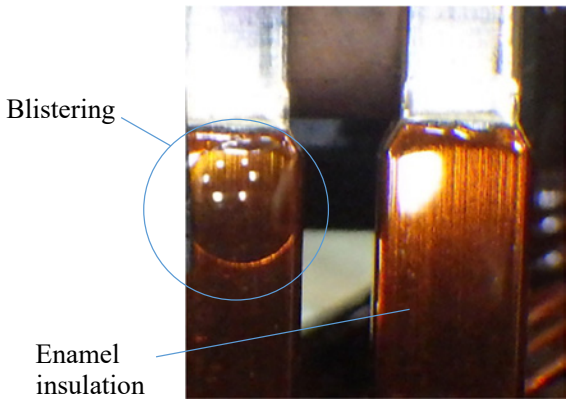


Fig. 4 Blistering

To guarantee an adequate breaking strength, the welded points should be strengthened by applying a large amount of energy during welding. In contrast, to suppress blistering, input heat energy must be suppressed to minimize the thermal effects on the enameled part. It is essential to balance welding conditions that satisfy these two opposing conditions.

## 4. Determination of welding equipment specifications

### 4.1 Specifications for high productivity

As described in 3.1, repeating the terminal clamping operation for each contact point does not achieve a production speed comparable to laser welding. Terminal clamping has the following three purposes and is required for flat wire welding.

<Purpose of terminal clamp>

(1) Alignment: To align the busbar terminals with the stator terminals and tightly attach them together.

(2) Supply of electric current: To cause contacts to the terminals to be welded so that a welding-current circuit is formed.

(3) Heat removal: To absorb weld heat before it reaches the enameled part and suppresses blistering.

In order to ensure reliable terminal clamping and minimize the machine operation time for clamping, a jig that simultaneously clamps all welding points (24 locations) (hereinafter referred to as the "clamping jig") was developed and used. In addition, the operation time for terminal clamping can be reduced significantly by placing the clamping jig outside the TIG welding machine so that it can be assembled and disassembled outside the welding machine.

Fig. 5 shows a diagram of the clamping jig developed in this study. The jaws that clamp the terminals are arranged radially on a disk-shaped base plate, and a spring is used to provide a clamping force to slide each jaw individually. (A patent application for this technology has been filed with the Japan Patent Office.) [(1)]

Furthermore, the clamping jig was designed according to the shape of each stator model and was stocked upstream of the welding machine, which enabled the random continuous production of five workpiece models.

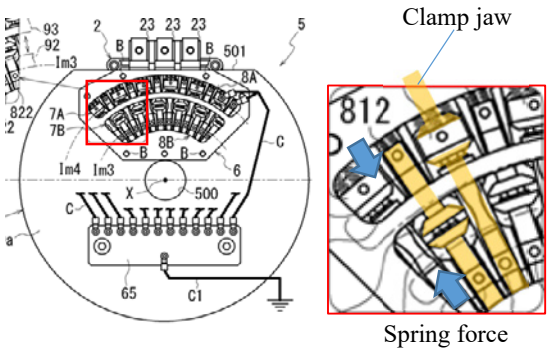


Fig. 5 All terminal simultaneous clamping jig

In addition, the operation step [2] Touch in Fig. 3 was eliminated to shorten the welding time. The role of the operation step is to maintain a constant height and distance between the welding terminal and the welding electrode. To guarantee this distance, a 3D camera was placed inside the welding machine. The camera takes pictures of the terminal position before welding, the terminal height is calculated, and the calculated value is fed back to the electrode height during welding.

As a result of using the above countermeasure, the torch is moved as shown in Fig. 6 during welding, which eliminated the time loss.

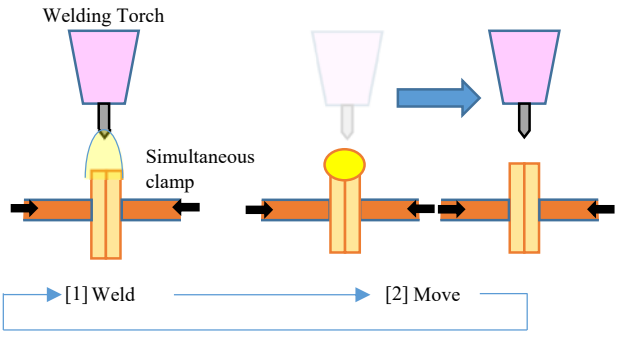


Fig. 6 Newly proposed terminal clamp

### 4.2 Specification for high quality

In the present busbar welding, all 24 terminals are welded to complete a single product. As described in 3.3, the precision of welding positions is important to enable a balance between weld strength and blister suppression. However, the position of the terminals in the component is determined by the position of the busbar, which is a rigid component. Hence, it is necessary to fine-tune the coordinates of the welding position for each component and each welding point.

To guarantee the optimal welding position for each component, the 3D camera mentioned in 4.1 was utilized. The system feeds back the detected terminal location to the welding position in terms of not only height but also X–Y coordinates.

The camera captures images as shown in Fig. 7. The 3D data image in Fig. 7a) is used to determine the shape and position of the terminal in the two-dimensional (2D) image, and the optimum welding point is then calculated and specified, as shown in Fig. 7b). The color in Fig. 7a) represents the height of the object; thus, the system was designed to also guarantee the appropriate welding height.

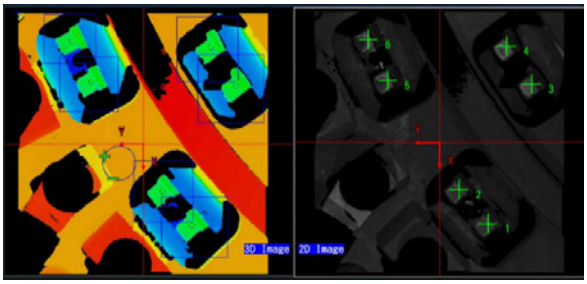


a) 3D image b) Welding position setting

Fig. 7 3D camera data

## 5. Status of the application for mass production

### 5.1 Pre-mass production issues and countermeasures

The trial production at this equipment found that the terminals were melted, the molten balls were unevenly distributed, and no bonding occurred between the terminals, as shown in Fig. 8.

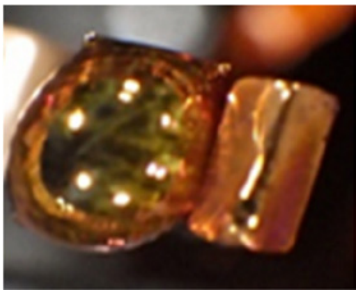

a) Upper view

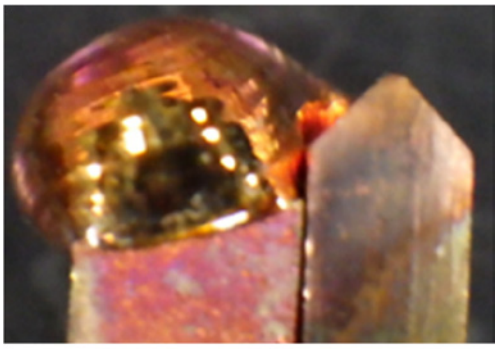

b) Side view

Fig. 8 Welding defect

This phenomenon, which is called “two-balls,” was observed and analyzed using a high-speed camera to detect the behavior of molten copper during welding. It was found to be caused by an imbalance in the magnetic field generated by the welding current, which attracts molten copper in a specific direction owing to the difference in electromagnetic force. Based on this, a control measure was designed so that the current flows evenly in the clamp. As a result, the two-ball phenomenon was suppressed.

### 5.2 Applications for mass production

After addressing the productivity and quality issues, the equipment was launched and mass production commenced in FY2025 (Fig. 9). The equipment met the target welding-speed, and the productivity was shown to be comparable to that of laser welding (Table 2).

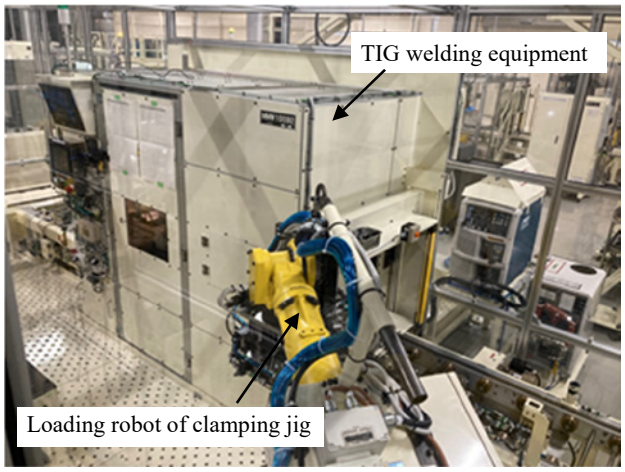


Fig. 9 TIG welding machine

Table 2 Comparison with JATCO welding method

| | Laser welding | TIG welding |
|---|---|---|
| Quality (Q) | × Spatter is generated | ○ No spatter |
| Cost (C) | × Welding machines are expensive | ○ Welding machines are inexpensive (approx. 1/5) |
| Time (T) | ○ High welding speed | ○ Production cycle time is the same as for laser welding |

## 6. Summary

The TIG welding equipment is currently used for mass production. Although some problems have occurred, we have solved all of them. In solving these problems, we realized the importance of analyzing phenomena in accordance with fundamental principles, such as the basic laws of electric circuits, analysis of heat transfer around welding points, and the structure and deterioration analysis of clamping fixtures.

It is expected that welding and joining methods will be further expanded for electrified units in the future. We will use the experience gained from this project to contribute to the future of electrified units.

## 7. References

(1) Kiyoto Tamura, Daisuke Hitokoto, Tatsuya Ishikawa, Masashi Kajita: A clamp jig, Patent Application 2024-038513, 2024.

■ Authors ■

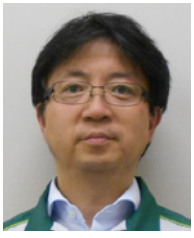

Daisuke HITOKOTO

Kouki OKUI

Wenqiang HE

# Development of Next-Generation Gear-Machining Line for Electrification

Yuta INOUE* Hidekazu HIOKI* Masahiko NATSUME*

## Abstract

In recent years, the automotive industry has been rapidly shifting from conventional gasoline-powered vehicles to electric vehicles, such as electric cars and hybrids, and the business environment is changing rapidly. To cope with this change, the conventional production system was replaced with a shop production system, in which each process is performed individually. The new system enables a company to respond flexibly to fluctuations in the number of units produced, increase the efficiency of capital investment, and shorten the production preparation period. In this paper, we report on this development.

## 1. Introduction

In line with the shift to electrification in the automotive industry, JATCO has transformed from an existing production system centering on a continuously variable transmission (CVT) to electrification (EV and HEV). In addition to changes in the external environment, such as environmental regulations and policy support caused by progress in electrification, many new companies are entering the market. Therefore, in the production of transmissions (drivetrain components), there is a need to respond to fluctuations in production volume, adapt to diverse customer specifications, and secure cost competitiveness, which is different from the past.

JATCO's production system is based on its JATCO Excellent Production System (JEPS)[(1)], which aims to improve competitiveness and contribute to profitability. In JEPS, the conventional production method (synchronous production line) is regarded as the ideal production system. However, it cannot respond flexibly to changes in production volume. Consequently, it is difficult to fully respond to customer needs, such as investment plans and delivery dates. Additionally, it is necessary to increase cost competitiveness by effectively utilizing existing equipment to machine CVT parts. To solve these problems, a new production system was developed and tested.

## 2. Problems of synchronous production lines

Figs. 1 and 2 show the problems associated with synchronous production lines. The vertical axis indicates the number of units produced, the horizontal axis indicates the year, the black line indicates the conventionally planned number of units, the red line indicates the projected number of units, reflecting fluctuations in the supply of electrified parts, and the blue line indicates the conventional line capacity.

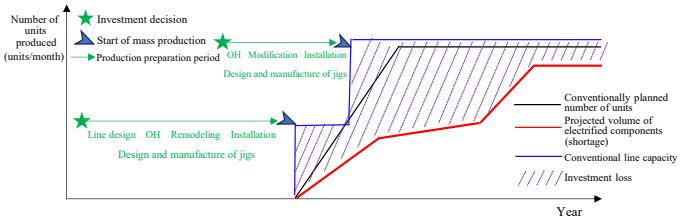


Fig. 1 Demand v.s. Line capacity (Demand decrease)

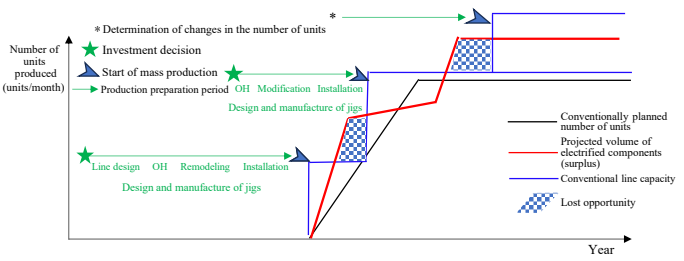


Fig. 2 Demand v.s. Line capacity (Demand increase)

*Machining Process Engineering Section No.2

The synchronous production line has a long production preparation period (green line) and numerous units per line. Therefore, when the number of units falls short of the planned number (Fig. 1), there is a surplus in line capacity, resulting in an investment loss (diagonally lined area). However, when the number of units exceeds the planned number (Fig. 2), the line capacity cannot be increased over time, resulting in opportunity losses (cross-hatched area). To address these problems, we studied a production system that minimizes excess line capacity and shortens the production preparation period.

## 3. Study of new production methods

In response to the transition to electric power, JEPS has maintained the philosophy of synchronous production and, simultaneously, has been overhauled using synchronous production in a more flexible way to systematically stock inventory items. This makes it possible to select a production system that can achieve line capacity and stability under changing environments.

Based on this strategy, manufacturing processes with similar characteristics (turning, gear cutting, grinding, etc.) are grouped together, and their smallest units are defined as a “shop.” A production system that provides inventory between these shops can increase the production capacity in small increments. Fig. 3 shows an overview of the conventional synchronous and shop production lines considered in this study.

In a synchronous production line, each process is connected in series such that there is little or no inventory and the flow between processes is smooth. The capacity of each line must be large to match the capacity of each process. To increase production capacity, a similar production line must be added. The capacity N of the entire line is determined by the capacity of the process with the smallest capacity in the line (the finishing process in Fig. 3).

Conversely, in a shop production line, each process is organized as an independent shop with inventory between them so that the production capacity can be increased on a shop-by-shop basis. In this example, the capacity of the finishing shop is 0.5 N, which means that the line can be operated as a production line with a capacity of 0.5 N.

If a finishing shop of 0.5 N is added, a lathe shop with a capacity of 0.75 N defines the line capacity. Therefore, a shop production line can increase its capacity by adding shop units. Hence, the line capacity can be increased in small increments to avoid creating excess line capacity. In addition, because capacity can be increased by shop units, the production preparation period can be expected to be shortened.

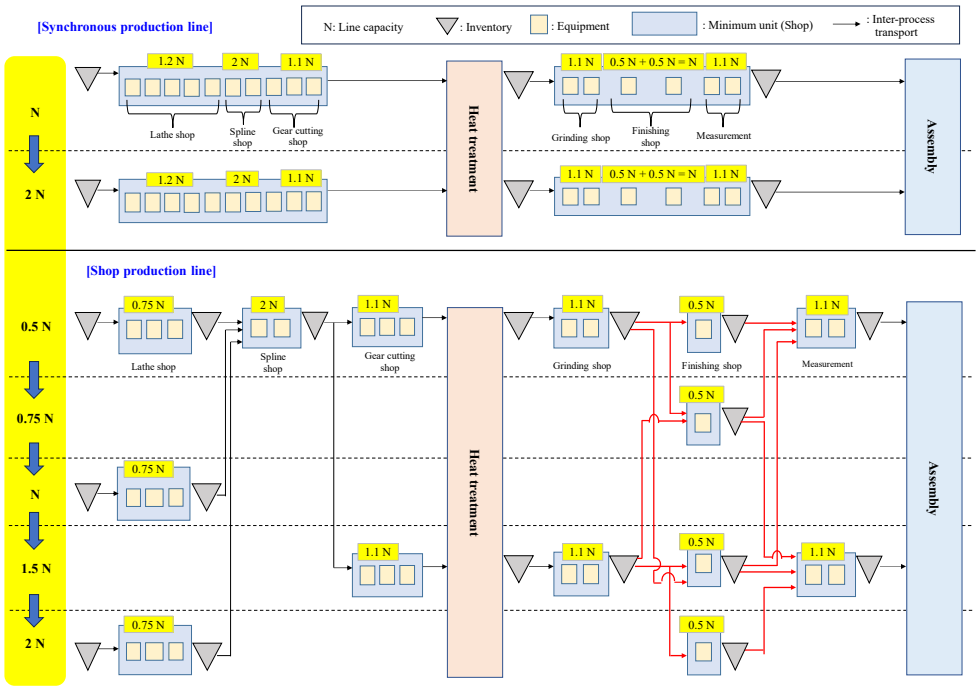


Fig. 3 Differences between Synchronous Production Lines and Shop Production Lines

## 4. Initiatives for using a shop production line

As described in Section 3, a shop production line can be expanded using units of equipment and shops, thus increasing its capacity in small increments. However, to use a shop production line, it is necessary to solve problems such as the increased complexity of inventory management and increased workload of inter-process transportation. This chapter explains the efforts to solve these problems.

### 4.1 Design, management, and operation of inventory

In a synchronous production line, inventory exists only during the final process. However, in a shop production line, the inventory is held between shops. In the present example, the number of inventory locations was approximately three times larger (Fig. 3), complicating the inventory management. To address this issue, a new inventory management method was developed.

#### (1) Designing the optimum quantity of inventory

In a shop production line, it is important to avoid stopping at the shop with the longest cycle time (called the "neck shop" . For this purpose, there must be an inventory of the front-end process. The concept of optimum inventory is illustrated in Fig. 4.

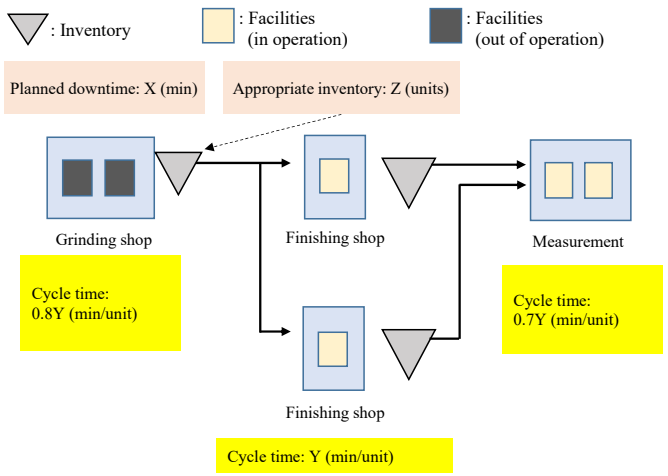


Fig. 4 Model for calculating the optimal inventory

Assuming that the cycle time of the finishing shop, which is the neck shop, is Y (min/unit), the planned downtime of the grinding shop, which is the process before the neck shop, is X (min), and the appropriate inventory is Z (units), the relationship between them can be expressed as follows:

Z (units) = X (min) / Y (min/unit)

The downtime X (min) is defined as the longest duration of planned stops, such as the model setup and tool change. Even when the grinding shop is stopped, the finishing shop, which is a bottleneck shop, is not stopped because inventory has been supplied to the finishing line. The required number of inventory units other than in the neck shop is defined as the standard number of packages (SNPs) of the cart. The operation of the part cart is described in (2).

#### (2) Methods to transport inventory

In a shop production line, the production sequence and processes vary widely, making the transport flow line complex (red line in Fig. 3). Therefore, if the conveyor transport method is used in synchronous production lines, setting up transportation routes and operating transportation onsite becomes difficult. To solve these problems, transportation by car has been investigated. The advantages of the cart transportation method are as follows:

Flexibility: Carts have no restrictions on route setting, and routes can be easily modified.

Investment and cost: Initial investment and running costs are lower compared to conveyors and production preparation period can be shortened.

Inventory management efficiency: Inventory can be managed on a cart, eliminating the need for refilling and facilitating easy transportation.

### (3) Methods to manage the optimum inventory number

In inventory management, when the number of items in stock exceeds the optimum number, inventory costs increase, whereas when it falls below the optimum number, the neck shop stops and productivity declines. Therefore, maintaining an optimal number of inventories is important. Because the optimum inventory number can be maintained by controlling the number of carts, the appropriate inventory number was set by rounding Z (units) as a multiple of the SNP of the carts. Overstocking was prevented by managing each cart at a fixed quantity and position between shops and by stopping the grinding shop when the number of carts reached a set value.

## 4.2 Implementation of an automated transport system

As described in Section 4.1, the shop production line has complex transport flow lines because of the inventory stocking between shops. Transportation using a conventional manual cart may result in lower work efficiency, higher labor costs, and quality risks such as part mix-up. Therefore, an automatic transfer system was introduced to stabilize and improve the efficiency of transportation operations.

### (1) Selection of transport methods

The specifications for automatic cart transportation were studied for autonomous mobile robot (AMR) and automated guided vehicle (AGV) types. The carts were transported between shops by under-cart crawling, towing, or lift-up. AMRs can move freely without being tied to a predetermined route. However, it is necessary to install sensors, AI control, and an integrated system. In this study, AGVs were selected because of their high cost advantage. Moreover, the route design was possible for AGVs owing to the fixable transportation route, and the cost of obtaining new AGVs could be eliminated by reusing the AGVs already owned by the company.

### (2) Design of AGV path

As described in (1), the inventory between shops was loaded onto carts, which were transported by AGVs. To maintain uninterrupted production, a cart carrying parts must always be present in the downstream shop. In addition, the use of a single cart between two shops causes shop downtime during the replacement of carts. Therefore, it was designed to provide space for two carts between the shops. Furthermore, because it is important not to stop at the neck shop, the transport route of the AGVs was designed as shown in Fig. 5. When the cart in the finishing shop becomes empty, the AGV swaps it with the cart in the grinding shop (Fig. 5 [1]). When two carts are loaded with parts in the finishing shop, the carts in the grinding shop are transported to the planned stock yard (Fig. 5 [2]). The inventory in the stock yard is supplied to the finishing shop when the grinding shop stops (Fig. 5 [3]). Thus, the downtime loss in the finishing shop, which is a bottleneck shop, can be minimized, enabling uninterrupted production and stocking.

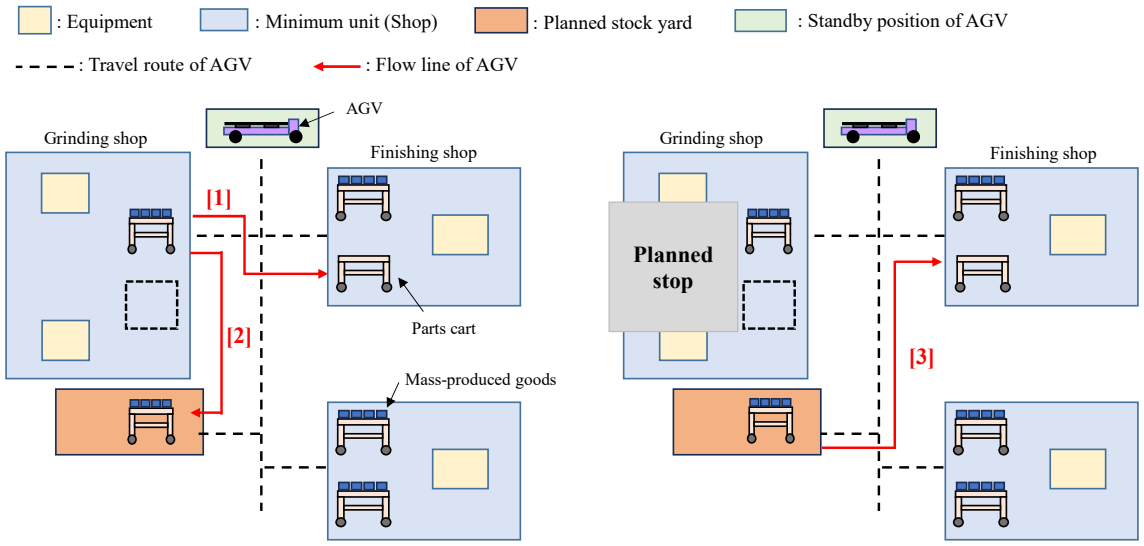


Fig. 5 Diagram of AGV and inter-shop parts cart

### (3) Linking of AGVs and robots

To continue uninterrupted production, carts must be precluded from being on the neck shop when empty. Therefore, it is necessary for the AGVs to automatically detect the state of the cart (full, empty, etc.) and link the cart with the in-shop transfer robot. To detect the state of the cart, an imaging device is installed on top of the cart. Each time the robot picks up a part on the cart, the state of the cart is imaged. When the cart becomes empty, information is transmitted from the in-shop transfer robot to the AGV, preventing the cart in the neck shop from becoming empty.

In addition, a cooperative, rather than industrial, robot was used as the in-shop transfer robot to reduce the downtime loss during the changeover of carts. When an AGV enters a shop, industrial robots cannot distinguish the AGV from the worker, causing the equipment in the shop to stop for safety reasons and resulting in downtime loss when replacing a cart. However, cooperative robots can continue production even when changing carts, thereby reducing the downtime.

The actual automatic transfer system introduced is described next. Fig. 6 shows the cart transport specification described in "(1) Selection of transport method." Fig. 7 shows the imaging equipment and cooperative robot described in "(3) Linking of AGVs and robots."

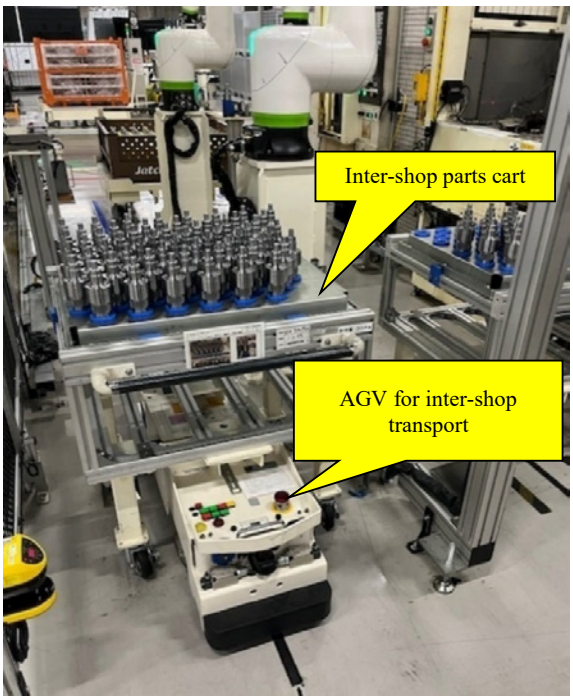


Fig. 6 Parts cart transport using AGV

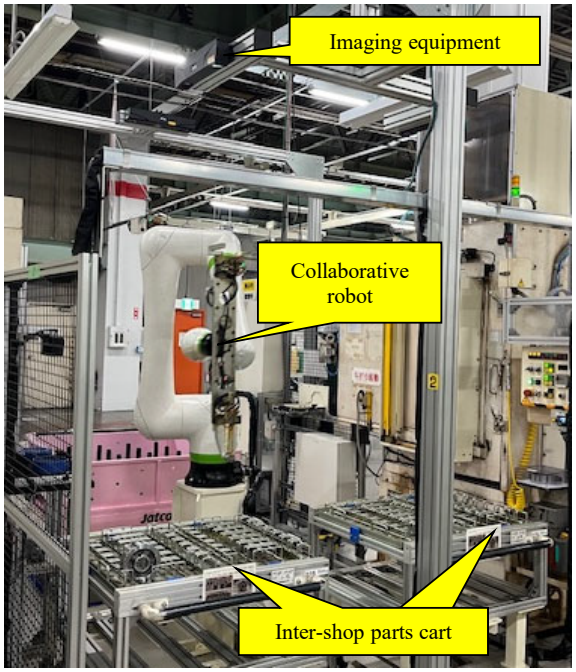


Fig. 7 Parts cart detection camera and collaborative robot

## 5. Confirmation of effectiveness

For a synchronous production line, when the number of units falls short of the planned number, there is a surplus in line capacity, resulting in a large investment loss (diagonally lined area). The investment loss (diagonally lined area) can be reduced using the shop production line, which can keep up with the change in the number of units (Fig. 8).

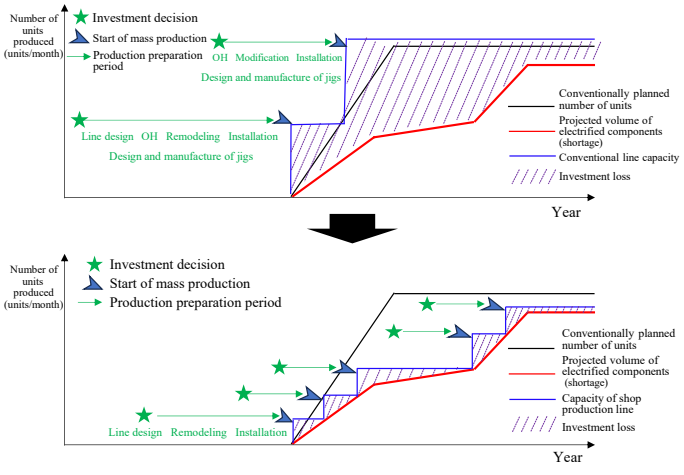


Fig. 8 Effect of shop production line, when the number of units decreases

In addition, in the case of a synchronous production line, when the number of units exceeds the planned number, the line capacity cannot be increased over time, resulting in opportunity losses (cross-hatched areas). However, using a shop production line shortens the production preparation period and reduces the risk of opportunity loss (Fig. 9).

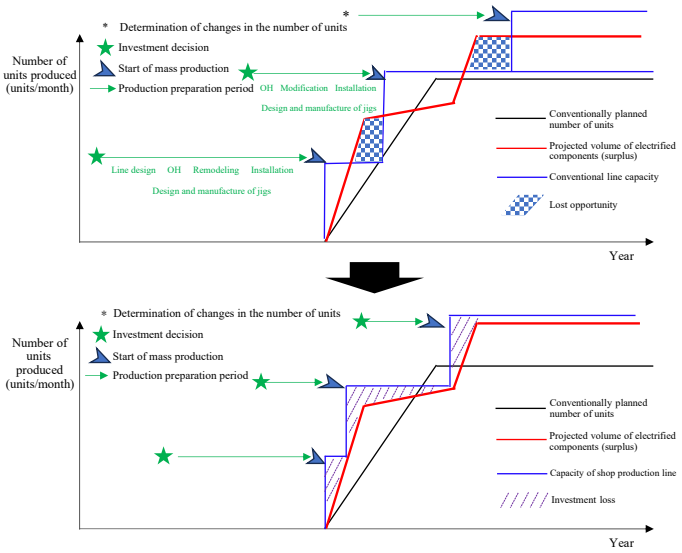


Fig. 9 Effect of shop production line, when the number of units increases

## 6. Discussion

In this study, a shop production line was introduced to overcome the inability of a synchronous production line to respond to fluctuations in production volume, thereby strengthening its ability to respond flexibly and shortening the production preparation period. This enabled the company to build a foundation for a production system that can respond to environmental changes associated with the transition to electrification.

Although a pilot line is effective for launching new parts, it is also useful for accommodating changes in production volume during production scale-up. Therefore, the use of synchronous production lines may not lead to major problems. In this regard, the shop production line is not always the optimal production system. In the future, we will develop a system that allows for the selection of appropriate production methods.

## 7. References

(1) Koji Watanabe and Masahiro Matsumoto: Global deployment of the JATCO Excellent Production System, JATCO Technical Review No. 14, pp. 65-70, (2015).

■ Authors ■


Yuta INOUE


Hidekazu HIOKI


Masahiko NATSUME

# Front-loading Quality Assurance for Noise and Vibration of Electric Powertrains

Kyohei OKAMOTO*

## Abstract

In recent years, the automotive industry has seen rapid progress in electrification amid the global trend toward carbon neutrality. The replacement of internal combustion engines with motors as power units has dramatically improved noise reduction in vehicles. However, this has resulted in the emergence of a new issue, in which occupants can easily detect faint sounds and vibrations that were previously masked by engine noise. This paper describes a front-loading quality-assurance approach developed to prevent noise and vibration, and achieve outstanding quietness in our first fully developed electric powertrain.

## 1. Introduction

In the past, our company's quality assurance in relation to noise and vibration (hereinafter referred to as "NV") from the transmissions for engine-powered vehicles was based mainly on an approach wherein the chassis and gears were first designed based on target NV values for that vehicle and the success in reaching those target NV values was checked using a single powertrain unit. For large vibration sources such as internal combustion engines, this approach is sufficient to guarantee NV quality. Thus, the main purpose of the NV evaluation using a vehicle was to conduct replication tests to identify the causes of problems only after they became apparent.

However, vehicles equipped with electric powertrains have no large noise sources such as internal combustion engines. Hence, there is a greater likelihood that occupants will notice faint NV, which have not been a problem in the past. Our electric powertrain has a structure that integrates a motor and an inverter, in addition to a gearbox. Thus, it has multiple NV sources, including the vibration of each component and resonance with the surrounding components. Conventional approaches, in which problems are individually addressed after they become apparent, require major design modifications and additional countermeasures in the final stages of development, which are risky in terms of both cost and time. Therefore, as shown in Fig. 1, we constructed and applied a front-loading quality-assurance process that proactively identifies and addresses potential problems in the early stages of development.

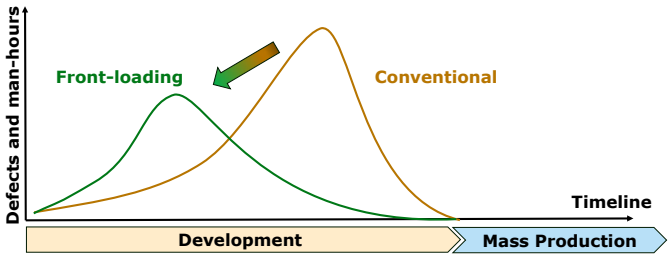


Fig. 1 Difference of conventional and front-loading

## 2. Development of a front-loading NV quality-assurance process

### 2.1 Systematic analysis of the factors that cause NV, using quality function deployment

Because NV are caused by a complex interplay between multiple factors, it is difficult to solve the root-cause of the problems by addressing each factor separately. Therefore, we used quality function deployment (QFD) to systematically organize causal relationships by translating customer-required quality into the characteristics of functional components.

*Corporate Quality Assurance Department

**Sample of QFD results (Differs from the actual results)**

| Customer requirements | ① NV defects | ② Target | ③ Allocated component characteristics | ④ Sensitivity | ⑤ Parameter |
|---|---|---|---|---|---|
| No noise that stand out from the background noise | Thumping noise when acceleration | ΔL ≤ 20dB | Shaft outer Diameter | By sensitivity line | Φ50＋0.500 |
| | | | Press-fit start shape | By sensitivity line | In drawing |
| | | | Bearing play | By sensitivity line | — |

Fig. 2 Sample of the results by QFD

Specifically, a team led by the development department used the following procedure to organize the causal relationships.

[1] Break down a customer-requirement quality ("no unpleasant noise and vibration") into potential NV occurrences.

[2] Set target values for each NV occurrence.

[3] Extract the quality characteristics of the functional components that affect the occurrence of NV.

[4] Evaluate the degree of correlation between the customer-required quality and quality characteristics using quality tables.

[5] Translate quality characteristics into specific values for control characteristics.

The control values were extracted from a desk study, as shown in Fig. 2. To verify these values using a vehicle, we performed the physical verification described below.

## 2.2 Physical verification needed at an early stage

Vehicles equipped with electric powertrains have no large noise sources such as internal combustion engines. Thus, there is an increased likelihood that even faint NV will be perceived by the occupants. In addition, NV are not caused by the electric powertrain alone but by the combined effects of multiple factors, such as the transmission path to the vehicle body, resonance of surrounding components, and acoustic characteristics of the cabin. Hence, it is extremely difficult to accurately predict the level of occupant perception based on desk studies. To guarantee the high quality desired for customers, physical verification of the final product (i.e., a vehicle) is necessary from the early stages of development. Therefore, in addition to verifying the problems identified by QFD, we decided to conduct large-scale physical verifications using prototype vehicles as the core of our quality-assurance process, with the aim of discovering difficult-to-predict NV occurrences. An actual physical verification scenario is shown in Fig. 3.

Fig. 3 Physical verification

| List the conditions | |
|---|---|
| **E.g.,)Condition** | **E.g.,) Driving pattern** |
| Speed | Maintain 60km/h |
| Torque | Maintain +80Nm |
| Temperature | Drive with 35℃ over |
| Throttle vol. | Keep 25% |
| Gradient | Brake at 10% slope |
| Acceleration | Slow acceleration |
| Deceleration | Deceleration with e-Pedal |
| Steering | Full steering |
| Shift | Shift D to N while driving |
| Special | Repeat acceleration and deceleration with extremely low torque |

**Combine conditions for efficiency**

- **-40Nm deceleration after maintaining 60km/h**
- **Full throttle with 35℃ over**
- **Step on the accelerator quickly with 10% gradient**

Fig. 4 Part of the driving pattern

## 2.3 Design of driving patterns to detect all NV occurrences

To detect all of the potential problems, it was necessary to design a driving pattern that covered all of the possible ways in which customers drive. We designed a driving pattern that could be used to evaluate potential NV problems specific to electric vehicles, by drawing assumptions about the NV occurrence mechanisms from the QFD results. Specifically, as shown in Fig. 4, in addition to the conventional basic driving patterns, we included acceleration controls such as sudden starts and rapid acceleration, frequent changes in the regenerative braking strength, and fine torque fluctuations to detect motor noise and gear backlash noise. In addition, we included various driving conditions expected in real situations, such as driving in urban areas, on highways, in traffic congestion, and on mountain roads. Thus, we could evaluate NV occurrences that are difficult to detect under a single condition.

Furthermore, recognizing the importance of the constraints related to time and the number of prototypes, we included multiple conditions in a single driving pattern, thereby developing a holistic driving pattern that could detect all of the NV occurrences while minimizing the driving distance and time, even with limited evaluation resources.

## 3. Results of applying the front-loading approach

By applying the front-loading quality-assurance system, dozens of NV problems were identified that could not be predicted in the desk study. All these issues were confirmed and addressed in the early stages of development. Consequently, no rework was necessary in the final stages of development.

Fig. 5 shows examples of NV occurrences analyzed at four levels: passenger perception (1), vehicle vibration (2), powertrain vibration (3), and component characteristic values (4), which were visualized as a series of cause-and-effect structures. Each quadrant is explained as follows.

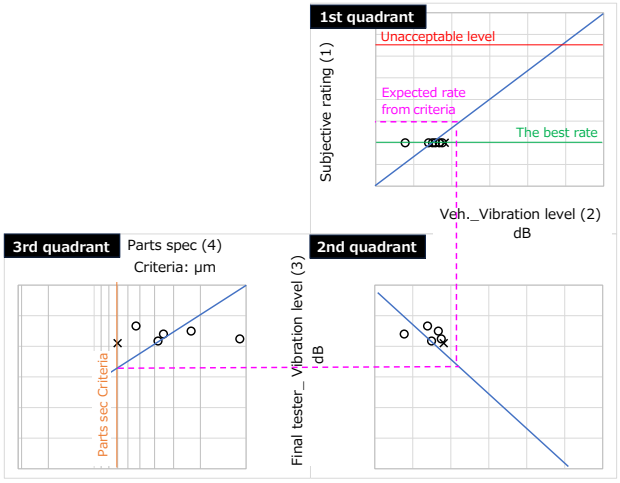


Fig. 5 Analysis results of acquired data

The first quadrant shows the relationship between the sensory score for the occupant perception (1) and vibration value measured in the vehicle (2). The occupant perception was quantified as a score. In this quadrant, no NV occurrences were perceived by the occupants, and all NV occurrences received the highest score. Therefore, there was no correlation between the occupant perception level and vehicle vibration.

The second quadrant shows the relationship between the vibration values measured on the vehicle (2) and the vibration values measured at the F/T (final tester: on-board NV assurance facility used during the manufacturing process) (3). A positive correlation was observed between vehicle vibration and F/T

vibration values. This indicates that the vibration values measured on the vehicle reflect the F/T results, that is, the vibration behavior of the electric powertrain itself.

The third quadrant shows the relationship between the vibration values measured by the F/T (3) and the characteristic values of the components obtained by QFD (4). No correlation was observed between the F/T vibration and component characteristic values. This was because the vibration level was suppressed to a certain low level by the control of the characteristic values of components and thus it was masked by the surrounding vibration.

The above results indicate that the vibration level caused by the electric powertrain was relatively small compared to the overall vibration level of the vehicle and was masked by other vibrations in the in-vehicle environment. Thus, no NV occurrence was perceived by the occupants, as indicated in the first quadrant.

The occupant perception level was estimated based on the sensitivity line established from the characteristic values of the components. As indicated by the dashed line, even when an electric powertrain with the upper tolerance limit of the components was used, the NV level was lower than the occupant perception threshold. The data measured when using the worst specifications for the powertrain, which was a product that used components with the upper tolerance limits, are shown as X in Fig. 5. The results physically verified that the powertrain did not reach the occupant perception threshold, even when using the powertrain with the upper-limit specifications.

## 4. Discussion

By organizing the characteristic values of the components, powertrain vibration, vehicle vibration, and occupant perception level as a streamlined causal structure, we established a process for estimating the occupant perception level from component specifications. It is believed that this process enabled the verification of the validity of the target NV values at the design stage.

In addition, by conducting front-loading quality assurance based on physical verification in the vehicle, it has become possible to identify NV problems in the early stages of development and implement early countermeasures, significantly reducing the risk of design changes in the final stages of development. This approach was demonstrated to be effective for products with a wide range of NV sources, such as electric powertrains.

## 5. Conclusion

This approach enabled us to identify and address potential quality issues thoroughly during the development phase, resulting in the development of a full-scale electric powertrain with zero NV defects.

This method is sufficiently versatile to systematically evaluate the cause-and-effect relationships among factors that include the components, powertrain, vehicle, and occupant perceptions, and is also effective in the horizontal deployment of other products.

## 6. Summary

In the future, we will improve the NV-occurrence prediction accuracy by conducting further detailed analyses and compiling a database consisting of the large amount of vehicle evaluation data accumulated through this activity. We will also establish an analysis method that shortens the time needed for highly accurate NV quality assurance, thereby contributing to shorter developmental lead-times, lower costs, and higher quality.

■ Authors ■

Kyohei OKAMOTO

# Quantification of the Influence of Factors on Abnormal Austenite Grain Growth in Carburized Steel Parts for Drivetrain

Yasuo ITOU* Gou KATOU* Makoto MAEDA**

## Abstract

Carburized components produced via cold forging may exhibit abnormal austenite grain growth, resulting in diminished mechanical strength. While the qualitative factors influencing this phenomenon are recognized, their relative degrees of impact remain poorly defined. Consequently, this study utilizes test specimens simulating the component manufacturing process to experimentally elucidate the relationship between specific influencing factors and the resulting austenite grain size following carburization.[1]

## 1. Introduction

Carburizing, quenching, and tempering (hereinafter referred to as "carburization") is a widely utilized heat-treatment method for automotive drivetrain components to achieve requisite wear resistance and fatigue strength. However, reports indicate that the abnormal grain growth (G.G.) of austenite crystal grains during this heat-treatment process significantly reduces the mechanical properties of the components, thereby adversely affecting product life and reliability.[2] Previous studies have identified factors related to the occurrence of abnormal G.G., specifically citing precipitate distribution, strain during plastic forming, and heat treatment temperature conditions as primary factors.[3] [4] However, the interaction between these factors and their respective degrees of impact on G.G. remain inadequately understood in many instances.

Test pieces simulating cold-formed carburized components (hereinafter referred to as "TP") were employed in this study to identify the factors affecting the occurrence of G.G. and to quantify the degree of their influence.

## 2. Objective

Previous investigations on the occurrence of G.G. evaluated the influence of individual parameters by isolating each variable.[5] However, actual component manufacturing involves a multitude of concurrent parameters affecting G.G. Therefore, to effectively suppress G.G., it is essential to comprehensively investigate these variables and to quantitatively evaluate the specific impact of each parameter on G.G.

Furthermore, even when the influence of a factor is quantified, its utility is limited if the factor remains uncontrollable within the component manufacturing process.

Therefore, this study aims to identify parameters that allow for direct feedback into the manufacturing conditions and to quantitatively evaluate their respective impacts.

*Hardware System Development Department **Innovative Technology Development Department

## 3. Methodology

G.G. is a phenomenon resulting from transformations in metallic microstructures. Accordingly, factors related to the mechanism of G.G. and those influencing its occurrence were systematically categorized relative to each stage of microstructural change. Specifically, the analysis was divided into the following four steps, as illustrated in Fig. 1:

STEP 1: Relationship between G.G. and microstructure following carburization,

STEP 2: Relationship between microstructures after carburization and after cold forming,

STEP 3: Relationship between the cold-formed microstructure and the initial material microstructure and manufacturing conditions, and

STEP 4: Relationship between G.G. and parameters controllable during manufacturing.

In each step, a multivariate analysis was performed to examine the relationships between the objective and explanatory variables, allowing for the extraction of highly correlated parameters.

Finally, in STEP 4, the relationships between G.G. and parameters controllable within the manufacturing process were quantified via multivariate analysis.

This methodology facilitates a sequential analysis of the influence of microstructural changes across intermediate processes. Consequently, this approach provides a clear understanding of the degree of impact on G.G. exerted by controllable manufacturing parameters such as material properties and component manufacturing conditions.

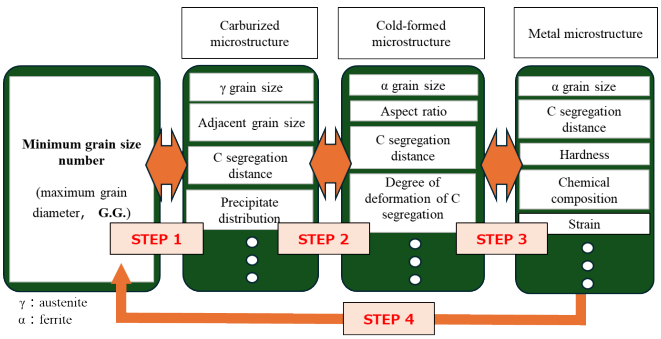


Fig. 1 Extraction and quantification procedure for G.G. influence parameters

## 4. Parameter extraction approach

### 4.1 Mechanism of G.G. occurrence

G.G. is a phenomenon that occurs to reduce the energy differential between adjacent grains, with grain boundary energy serving as the primary driving force.

However, the mechanism of G.G. occurrence depends not only on the grain boundary energy, but also on several extrinsic factors, including strain energy, thermal energy, and the G.G. inhibition energy provided by precipitates. To account for these combined effects, the influencing parameters associated with each energy factor were systematically extracted in this study.

### 4.2 Parameters related to grain boundary energy

Grain boundary energy, which is determined by crystallographic factors, is the intrinsic energy of the grain boundary itself.

The G.G. occurring during the carburization process is a phenomenon that mitigates the energy gradient resulting from differences in the grain boundary curvature. Therefore, under constant strain and thermal energy conditions, the occurrence of G.G. is primarily attributed to the grain size differential between adjacent crystals. From this perspective, parameters related to grain size and its distribution within the metallic microstructure were extracted in this study.

### 4.3 Parameters related to strain energy

Strain energy is the energy stored within a material during plastic deformation processes, such as cold forming. Strain energy directly affects the recrystallization and phase transformation temperatures during carburization and is an important factor controlling the behavior of G.G. Accordingly, parameters related to cold forming conditions and the resulting cold-formed microstructure were extracted in this study.

### 4.4 Parameters related to thermal energy

Thermal energy is the energy imparted to a material during heat treatment processes such as carburization. The magnitude of this energy significantly influences the growth behavior of crystal grains following recrystallization and phase transformation. To quantitatively evaluate this effect, the temperature conditions during carburization were extracted as critical parameters in this study.

### 4.5 Carbon concentration distribution

Variations in the carbon concentration in a material induce changes in the transformation temperature of the metallic microstructure and the formability of the material. Specifically, during cold forming processes, ferrite grains (hereinafter referred to as "$\alpha$ grains") situated around carbon segregation sites (hereinafter referred to as "C segregation sites") tend to exhibit greater deformation and accumulate higher strain energy than those in regions devoid of C segregation. Therefore, parameters related to the microstructural properties surrounding C segregation sites were extracted in this study.

### 4.6 Parameters related to grain-growth inhibition energy

Fine dispersion of precipitates at grain boundaries can effectively suppress G.G. Precipitates with diameters of 20 nm or less are reportedly effective in suppressing G.G.[6] Accordingly, parameters related to the precipitate size distribution were extracted in this study.

Following these principles, the various energy factors involved in the mechanism of G.G. occurrence were systematically categorized, and the parameters influencing each energy factor were comprehensively extracted (Table 1).

Table 1 Extracted parameters

| | |
|---|---|
| **Material and forming parameters** | Hardness |
| | α particle size No. ave. |
| | α particle size No. σ |
| | C segregation width ave. |
| | C segregation width σ |
| | C segregation width ave.-σ |
| | C segregation interval ave. |
| | C segregation interval σ |
| | C segregation interval ave.-σ |
| | Chemical composition |
| | Shear strain |
| | Equivalent strain |
| **Post-cold forming and carburization parameters** | α particle size No. ave. in C segregation |
| | α particle size No. σ in C segregation |
| | α particle size No. ave. |
| | α particle Size No. σ |
| | Aspect ratio of α particles |
| | P-F angle |
| | L×Θ |
| | T×Movement distance |
| | Hardness ×C segregation movement distance |
| | C segregation interval ave. |
| | C segregation interval σ |
| | C segregation interval ave.-σ |
| | C segregation width ave. |
| | C segregation width σ |
| | C segregation width ave.-σ |
| | Carburizing temperature |
| **Post-carburization parameters** | γ particle size No. ave. |
| | γ particle size No. σ |
| | γ particle size area ratio (No. ≤ 5) |
| | γ particle size area ratio (No. ≥ 10) |
| | Area ratio of particle size No. ≤ 5 near C segregation |
| | Area ratio of particle size No. ≥ 10 near C segregation |
| | γ particle size No. ave around maximum γ particle |
| | γ particle size No. σ around maximum γ particle |
| | Distance from maximum γ particle to C segregation |
| | C segregation interval |
| | C segregation width |
| | Quantity of fine precipitates |
| | Precipitate size ave. |

## 5. Experimental methods

Experiments were conducted in this study using TPs that simulated the actual component manufacturing process to comprehensively investigate the variations in the metallic microstructure during the manufacturing process.

### 5.1 Specimen material

SCr420, as specified in the JIS G 4053 standard, was used as the specimen material. Three material production lots were used in the experiments to vary the states of the precipitates (Table 2).

Table 2 Chemical composition (mass%)

| Steel | C | Si | Mn | P | S | Al | N |
|---|---|---|---|---|---|---|---|
| A | 0.21 | 0.31 | 0.89 | 0.017 | 0.015 | 0.044 | 0.021 |
| B | 0.22 | 0.33 | 0.86 | 0.017 | 0.015 | 0.038 | 0.018 |
| C | 0.22 | 0.33 | 0.86 | 0.019 | 0.015 | 0.043 | 0.018 |

### 5.2 Material microstructure

As described in Section 4.5, the material microstructures influences the strain applied to $\alpha$ grains during cold forming. TPs with distinct metallic microstructures (Fig. 3) were produced by first machining the specimens into cylindrical $\phi 8 \times 12$ mm TPs, followed by heating them to the $\gamma$ single-phase region, and subsequently cooling them at varied rates (Fig. 2).

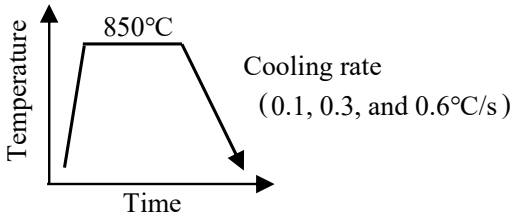


Fig. 2 Conditions for controlled microstructures

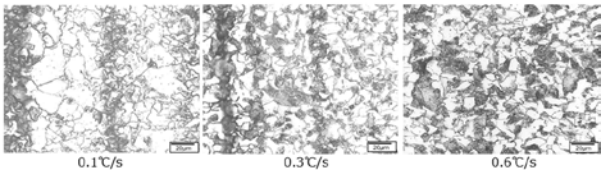


Fig. 3 Examples of controlled microstructures

### 5.3 Addition of strain energy owing to cold forming

Cold forming was performed via simple compression of the cylindrical TPs. The applied effective strain and shear strain were determined via finite element analysis. Furthermore, changes in the metallic microstructure relative to the varied strain distributions within the TPs were also investigated (Fig. 4).

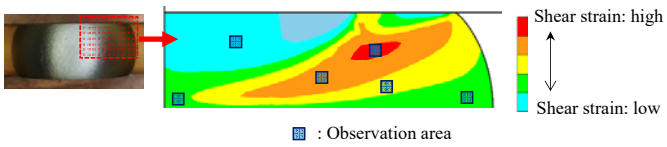


Fig. 4 Finite element analysis of strain distribution during compression testing

### 5.4 Addition of thermal energy by carburization

Three carburization temperatures were used in this study, namely, 950, 970, and 1,000°C. After holding the specimens at each temperature for a prescribed time, the specimens were oil quenched (Fig. 5).

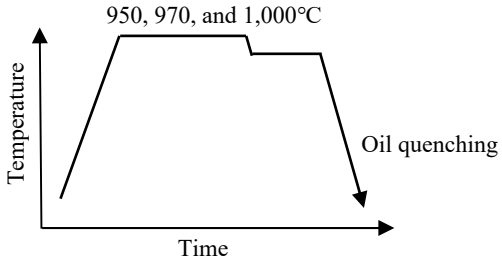


Fig. 5 Carburization Conditions employed in the study

### 5.5 Occurrence of G.G. and its relationship with each parameter

The metallic microstructure at each stage of the process was examined, and the parameters listed in Table 1 were quantified. In this study, the grain size of the metallic microstructure was determined by measuring the crystal grain size number (hereinafter referred to as "grain size No.") in accordance with the JIS G 0551 standard. This standard indicates that a larger grain size No. represents a finer crystalline grain size (hereinafter referred to as "grain size").

The metallic microstructure was examined, and factors related to the microstructure were quantified. This data was used to perform a multivariate analysis to evaluate the relationships between the objective and explanatory variables for each step illustrated in Fig. 1.

## 6. Results

### 6.1 Factors influencing G.G. during intermediate processes

#### 6.1.1 Relationship between G.G. and the microstructure after carburization (STEP 1)

As previously reported, G.G. is highly correlated with the metallic microstructure following carburization (Table 3, Fig. 6). Significant G.G. was observed near the periphery of the C segregation (Fig. 7), where the variation in the γ grain size was substantial. This indicates that G.G. was strongly influenced by the factors associated with the carburization process.

Table 3 G.G. parameters of carburized microstructure

| Objective variable name | $R^2$ |
|---|---|
| Maximum γ grain size number | 0.78 |
| Explanatory variable name | Standardized regression coefficient |
| Distance to C segregation in maximum γ grain | 0.50 |
| Area ratio of γ grains with size number < 5 near the C segregation | -0.31 |
| Average size number of the grains surrounding the maximum γ grain | -0.24 |
| Amount of AlN fine precipitates | -0.04 |
| Average diameter of AlN precipitates | 0.00 |

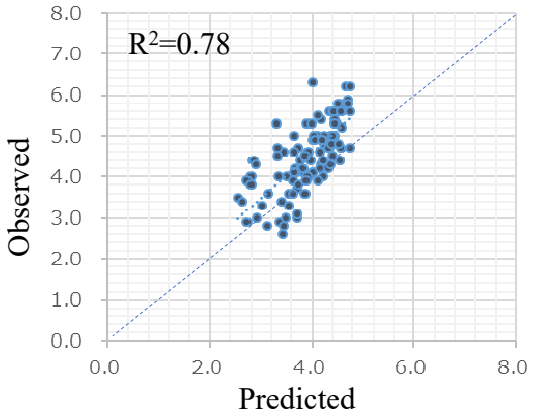


Fig. 6 Multivariate analysis results using carburized metal microstructure parameters (STEP 1)

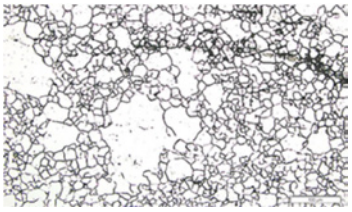

Fig. 7 An example of post-carburizing microstructure where G.G. occurs

#### 6.1.2 Relationship between the post-carburization microstructure and parameters after cold forming (STEP 2)

Among the parameters extracted in Section 6.1.1, those demonstrating strong correlation with the post-carburization microstructure include the average α grain size No. of the material and its variation, grain size No. following cold forming, distance to the C segregation, and deformation angle near the C segregation, the latter representing the crystal deformation degree. These were identified as the dominant parameters (Table 4).

The results indicate that the post-carburization microstructure influencing G.G. is related to both the inter-granular energy following cold forming and the strain energy accumulated during the cold forming process.

Table 4 Relationship between post-carburizing microstructure and parameters after cold forming

| G.G. correlated to the post-carburization microstructural parameters | Highly correlated post-cold-forming parameters | Standardized regression coefficient | $R^2$ |
|---|---|---|---|
| Average grain size number of the surrounding γ coarse grains (No. 4 and below) | Variation in the α grain size | -1.09 | 0.70 |
| | Average α grain size number | -0.43 | |
| Area ratio of crystals with an γ grain size number ≥ 10 near the C Segregation | Carburization temperature | -0.60 | 0.55 |
| | Average α grain size number | -0.49 | |
| | Variation of α grain size | -0.35 | |
| Distance to C segregation in the maximum γ grain | C segregation deformation angle | 1.69 | 0.34 |
| | C segregation interval | -0.47 | |
| Area ratio of crystals with an γ grain size number < 5 near the C segregation | C segregation deformation angle | 0.70 | 0.30 |
| | Carburization temperature | 0.54 | |
| | C Segregation interval | -0.36 | |

### 6.1.3 Relationship between the parameters after cold forming and the material microstructures and manufacturing parameters (STEP 3)

Among the parameters extracted in Section 6.1.2, those exhibiting a strong correlation with the post-cold-forming parameters were the α grain size No. of the material and its variation, width and interval of the C segregation, and shear strain (Table 5).

In STEP 3, the parameters associated with grain boundary energy and strain energy correlated with the post-cold-forming parameters influencing G.G., consistent with the findings in STEP 2.

Table 5 Relationship between parameters after cold forming and material microstructure and manufacturing condition parameters

| Parameters after cold forming | Highly correlated material factors | Standardized regression coefficient | $R^2$ |
|---|---|---|---|
| α grain size after cold forming | α grain size of the material | 0.82 | 0.67 |
| C Segregation interval after cold forming | C segregation interval in the material | 0.30 | 0.30 |
| Variation in the α grain size after cold forming | Variation in the α grain size of material | 0.52 | 0.29 |
| | C segregation width of material | -0.55 | |
| Deformation angle of C segregation after cold forming | Shear strain | 0.55 | 0.31 |
| | C segregation width of material | 0.18 | |
| Shear energy | Shear strain | 0.61 | 0.39 |
| | C segregation width of material | 0.33 | |
| Carburization temperature | Carburization temperature | - | - |

### 6.2 Relationship between G.G. and the manufacturing parameters that can be controlled (STEP 4)

Based on the microstructural analysis detailed in Section 6.1, the relationship between G.G. and the carburization temperature was examined by incorporating the temperature into the parameters extracted in Section 6.1.3. Consequently, the hierarchy of influence on G.G. was identified as α grain size No. > variation of the material α grain size No. > C segregation width > carburization temperature > shear strain (Table 6).

These results confirm that the occurrence of G.G. is influenced by grain boundary energy (material microstructure), strain energy (cold-forming conditions), and thermal energy (carburization temperature).

Table 6 Relationship between G.G., material structure and manufacturing parameters

| Objective variable name | $R^2$ |
|---|---|
| Maximum γ grain size number | 0.21 |
| Variable name | Standardized regression coefficient |
| Material α grain size number | -0.72 |
| Variation σ in the α grain size | -0.53 |
| Width of C segregation in the material | 0.43 |
| Carburization temperature | -0.35 |
| Shear strain | -0.34 |

## 7. Discussion

Among the parameters controllable within the manufacturing process, the α grain size No. (α grain size) of the material exhibited a high correlation with G.G. This relationship is speculated to result from the following phenomena:

[1] When the α grain size No. is large (indicating a fine α grain size), the resulting γ grain size following phase transformation is also fine. Therefore, even a minor differential in grain size promotes G.G. due to the high associated grain boundary energy.

[2] Finer grain sizes generally increase material strength and decrease deformation performance during forming. Therefore, when a material with fine grains, which is inherently more resistant to deformation, is cold-formed, a strain differential arises between the local fine-grained microstructure and the other regions in the microstructure, thereby promoting and G.G. This phenomenon is analogous to that described in Section 4.5.

Conversely, parameters related to precipitates were not identified as significant factors influencing G.G. in STEP 1 shown in Fig. 1 (Table 3). This may occur because, in cold-formed components subjected to substantial plastic deformation, the driving force promoting G.G. is more dominant than the inhibition energy provided by precipitates.

In this study, controllable parameters with significant impacts on G.G. were identified by evaluating the causal relationships with intermediate parameters in a stepwise manner, as shown in Fig. 8. However, the direct relationship between these identified parameters and G.G. exhibited a very weak correlation, as shown in Fig. 9 (results in Section 6.2, Fig. 10).

It is posited that this weak correlation stems from the omission of the causal relationships between the intermediate factors shown in Fig. 8. Therefore, in phenomena involving multiple microstructural transformations, the relationships between parameters at each stage must be considered to accurately predict the final microstructure.

As shown in Fig. 11, G.G. occasionally occurred under low-strain conditions rather than high cold-strain conditions, despite identical material properties and carburization temperatures. In this study, all relationships between parameters were modeled as linear; consequently, parameters characterized by nonlinear relationships, such as those indicated by the dashed lines in Fig. 12, were not extracted as highly important parameters. This likely explains why certain observed phenomena could not be elucidated solely through the identified parameters.

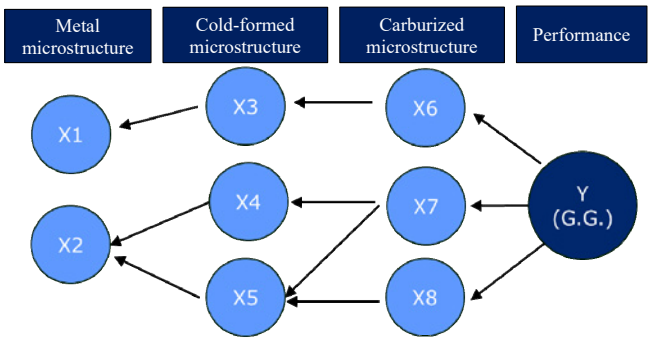


Fig. 8 Method for identifying the influencing factors

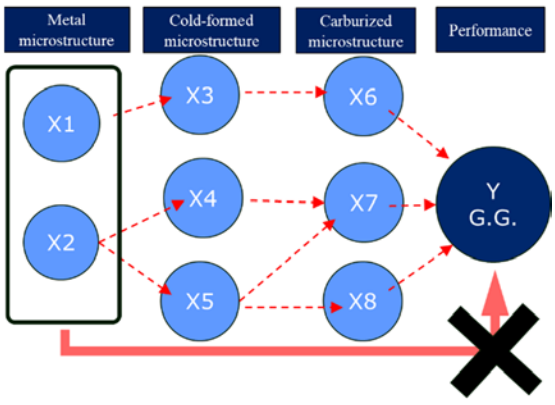


Fig. 9 Method for predicting the G.G.

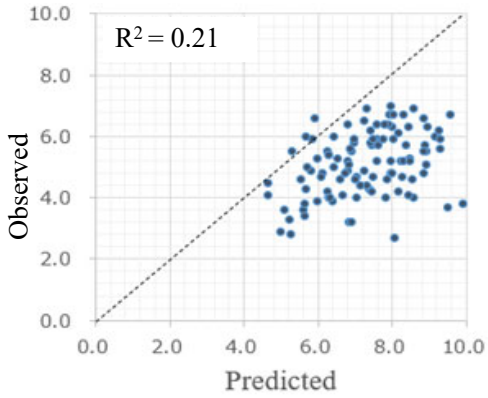


Fig. 10 Multivariate analysis results using material microstructure and manufacturing condition parameters (STEP 4)

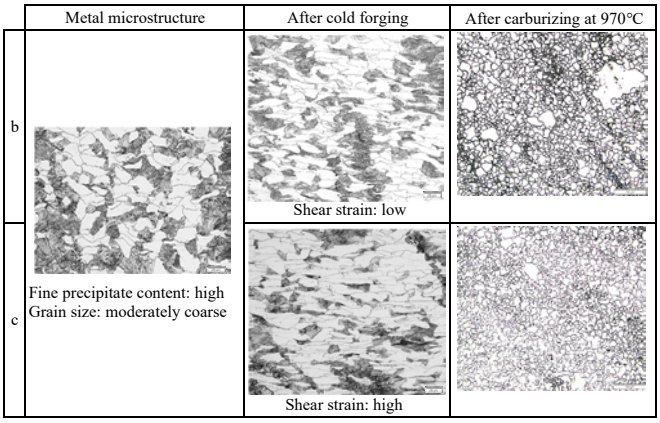


Fig. 11 Comparison of the pre- and post-carburization microstructures

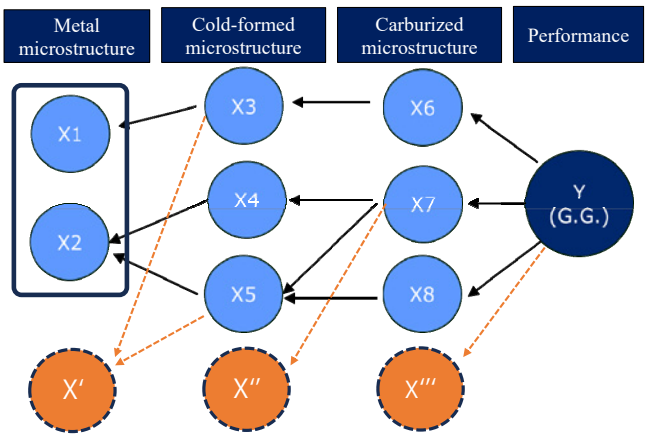


Fig. 12 Issues in the current influencing factor identification approach

## 8. Conclusion

The following findings were established in this study:

[1] The parameters affecting controllable G.G. within the component manufacturing process were extracted, and their respective degrees of impact were elucidated.

[2] The hierarchy of influence of the controllable influential parameters on G.G. was $\alpha$ grain size No. > variation in the $\alpha$ grain size No. > C segregation width > carburization temperature > shear strain.

[3] Examination of the direct relationship between the controllable parameters and G.G. revealed a weak correlation. This is attributed to the fact that G.G. involves a sequence of repeated microstructural transformations; consequently, correlations are significantly stronger when intermediate parameters and the synergistic combinations of parameters influencing these changes are considered.

## 9. References

(1) Yasuo Ito, Go Kato and Makoto Maeda: Quantification of the Influence of Factors on Abnormal Austenite Grain Growth in Carburized Steel Parts for Drivetrain, Proceedings of the 2025 Spring Meeting, The Society of Automotive Engineers of Japan, 2025, pp. 1–5, reprinted with permission.

(2) Tatsumi Urita, Kunio Namiki and Tomohito Iikubo: Electric Steelmaking, 59, 1, 33.

(3) Takeshi Fujimatsu, Morihiko Nakazaki, Shinji Fukumoto and Atsushi Yamamoto: Iron and Steel, Vol. 95 (2009), No. 2.

(4) Takeshi Fujimatsu and Kazuya Hashimoto: Sanyo Technical Report, Vol. 17 (2010), No. 1.

(5) Manabu Kubota and Tatsuro Ochi: Nippon Steel Technical Review, 378 (2003), 72.

(6) Naohide Kamiya, Yuki Tanaka and Ryohei Ishikura: DENKI-SEIKO, 89 (2018), 1.

■ Authors ■


Yasuo ITOU


Gou KATOU


Makoto MAEDA

# Prediction of Abnormal Grain Growth in Carburized Components Using Bayesian Networks

Yasuo ITOU* Gou KATOU* Makoto MAEDA** Takumi YOSHIDA***
Tsubasa YAMASHITA*** Shuhei KOJIMA*** Junya INOUE****

## Abstract

Abnormal grain growth, which leads to a decrease in the strength of carburized drivetrain components, is a complex phenomenon that is difficult to predict. In this study, we developed a method for predicting the occurrence of abnormal grain growth by constructing a Bayesian network, which was trained using test piece data to simulate cold forging based on the material properties and manufacturing conditions.(1)

## 1. Introduction

In recent years, the automotive industry is facing a strong demand for a stable supply of high-quality components with short development time to address CASE (Connected, Autonomous, Shared & Services, Electric). With a decrease in the number of skilled engineers and the ongoing digital transformation (DX) at manufacturing sites, efficient methods are urgently required to optimize manufacturing conditions.

Against this industrial background, the optimization of manufacturing processes and conditions using artificial intelligence (AI) has been attracting attention as an effective approach to simultaneously shorten the development time and stabilize product quality.(2) Based on these technological trends, our company has begun developing AI-based technologies to optimize manufacturing processes.

## 2. Themes and issues

Because drivetrain components are mainly associated with power transmission, they are carburized and tempered at high temperatures to ensure high strength. One of the concerns in this process is the grain growth (G.G.) of the steel crystals, which causes a reduction in component strength (Figs. 1 and 2). This phenomenon is caused by a combination of factors such as the metal microstructure, carburizing temperature, and plastic strain.(3)

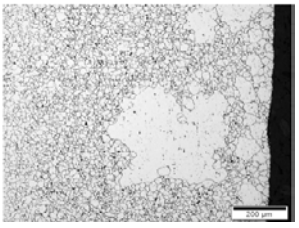

Fig. 1 Example of G.G.

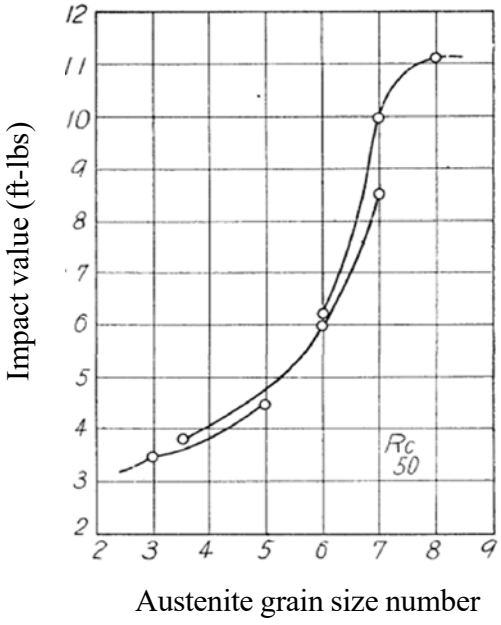


Fig. 2 Strength reduction due to G.G. (4)

*Hardware System Development Department **Innovative Technology Development Department ***MI-6 Ltd. ****The University of Tokyo

This makes prediction using a simple regression of the parameters difficult, making it necessary to predict by considering the variations in sensitivity that depend on a combination of parameters (Fig. 3).

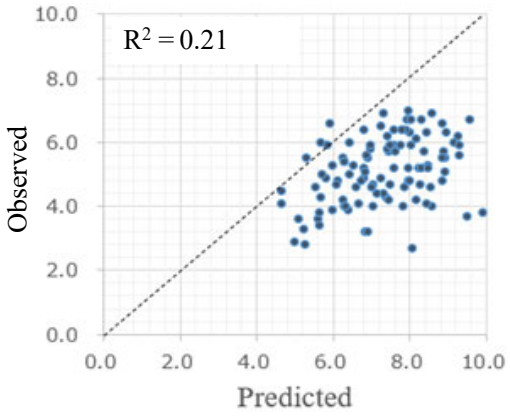


Fig. 3 Multiple regression analysis of post-carburization grain size number based on in-house evaluation test results

In a previous study, the quantitative effects of these parameters on the occurrence of G.G. were reported by varying only certain parameters.[5] However, because other parameters also vary in actual component manufacturing, configuring the component manufacturing conditions based on this previous study is difficult.

Therefore, we aimed to predict the G.G. occurrence using various combinations of multiple parameters that are varied simultaneously.

## 3. Methodology

In this study, AI was used to predict G.G. occurrence using various combinations of multiple parameters that were varied simultaneously.

The prediction of material properties using AI has been widely applied, mainly for polymeric materials whose properties are determined in a single process.[6] However, few examples of applications exist for predicting the properties of steel components that undergo complex microstructural changes during multiple processes.[7]

In conventional prediction models with simple AI usage, AI tends to learn the relationships between explanatory and objective variables without considering the relationships among explanatory variables. Hence, the prediction cannot adequately consider the effects of a combination of explanatory variables.

Therefore, we decided to use a probabilistic model (hereinafter referred to as a "Bayesian network") that directly represents the causal structure and reflects existing knowledge (Fig. 4).

We believe that this will enable us to conduct complex and diverse combinatorial studies and ultimately predict the occurrence of G.G.

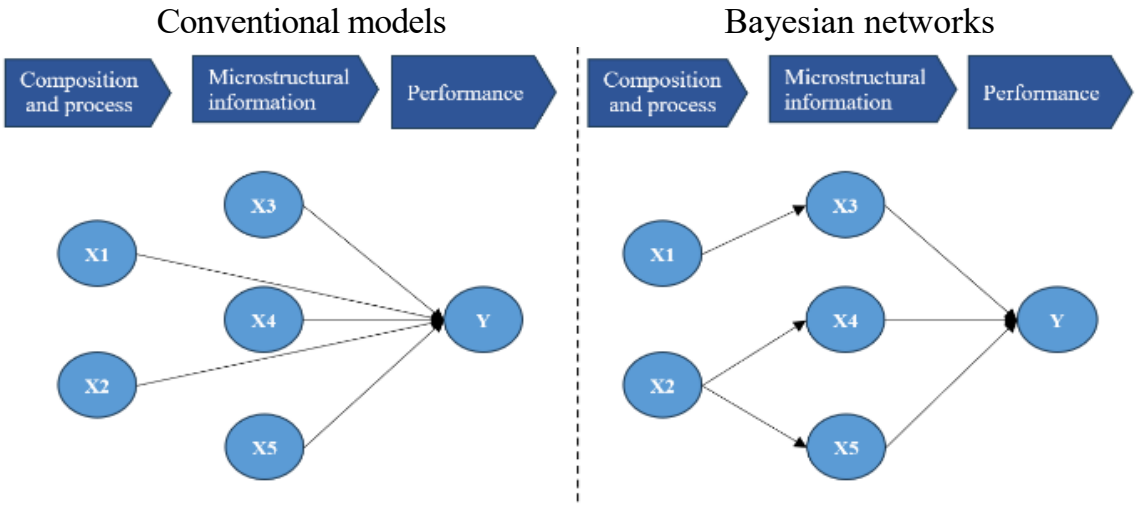


Fig. 4 Comparison between conventional prediction models and Bayesian networks

Generally, Bayesian networks assume a specific distribution, such as a normal distribution, when dealing with continuous values. Therefore, if the actual data deviate from this assumption, prediction accuracy may decrease. However, in this study, the problem was defined as a binary (discrete) classification problem of "whether or not G.G. occurs," thus obviating the need to deal directly with continuous-value data such as grain size. The largest grain size after carburizing was measured according to JIS G 0551, and G.G. occurrence was defined as a largest grain size of 5 or less after carburization.

With such discrete-value data, conditional probabilities can be modeled directly and computation can be performed efficiently without the risk of errors associated with distributional assumptions.

For this reason, we decided to use a Bayesian network based on classification.

## 4. Analytical procedure

Combination analysis and predictability evaluation utilizing AI were conducted using the results of test piece (TP) evaluations conducted in advance, by varying the parameters, thereby confirming the occurrence of G.G. The TP evaluation was performed by simulating actual component manufacturing, and each parameter was set considering the manufacturing range of the actual components.

In this study, using real data was expected to improve the prediction accuracy of G.G. occurrence without any supplemental AI learning.

To reflect the results of this study on actual component manufacturing, a model was developed to predict the occurrence or absence of G.G. using materials and process parameters that could be controlled during manufacturing.

### 4.1 Selection of influential parameters

Among the parameters identified as affecting G.G. in the preliminary TP evaluation, we selected those that correlated well with the largest grain size after carburizing.

Among the selected parameters, those that were collinear with the largest grain size after carburization were excluded (Table 1).

Table 1 Parameters affecting G.G.

Orange hatching: selected parameters

| | |
|---|---|
| Material and forging parameters | Grain size number ave. |
| | Grain size number σ |
| | Width of pearlite bands σ |
| | Width of pearlite bands ave.-σ |
| | Spacing of pearlite bands σ |
| | Spacing of pearlite bands ave.-σ |
| | Shear strain |
| | Effective strain |
| Post-cold forming and carburization parameters | Grain size number in carbon segregation ave. |
| | Grain size number ave. |
| | Grain size number σ |
| | Aspect raito |
| | Angle between pearlite and gerrite |
| | L×Θ |
| | τ×migration distance |
| | Hardness×migration distance of carbon segregation |
| | Spacing of carbon segregation ave. |
| | Spacing of carbon segregation σ |
| | Spacing of carbon segregation ave.-σ |
| | Width of carbon segregation σ |
| | Width of carbon segregation ave.-σ |
| | Carburizing temperature |
| Post-carburization parameters | Grain size number ave. |
| | Grain size number σ |
| | Area fraction of grains with grain size number 5 or less |
| | Grain size number around the largest grain ave. |
| | Grain size number around the largest grain σ |
| | Distance from the largest grain to pearlite bands |
| | Spacing of pearlite bands ave. |
| | Width of pearlite bands ave. |

### 4.2 Construction of a directed acyclic graph

Construction of a Bayesian network, requires that the relationships among the variables be represented.

A directed acyclic graph (DAG), which is the basis of the Bayesian network, was constructed based on the principles and relationships between the parameters obtained from the model. Because G.G. is caused by changes in the meta-microstructure during component manufacturing, the model was constructed step by step considering the changes in the microstructure (Fig. 5).

### 4.3 Discretization of variables

When dealing with Bayesian networks using classification, continuous values should be converted into discrete values.

Therefore, the data for the set of parameters were discretized and classified. Specifically, the parameter values after cold forming and those of carburizing conditions were used to obtain the values (thresholds) that would allow to roughly categorize whether the size of the largest grain was less than 5 after carburizing.

Similarly, threshold values were determined for the parameters of the material and cold forming conditions, to broadly classify them with respect to carburization (Fig. 6).

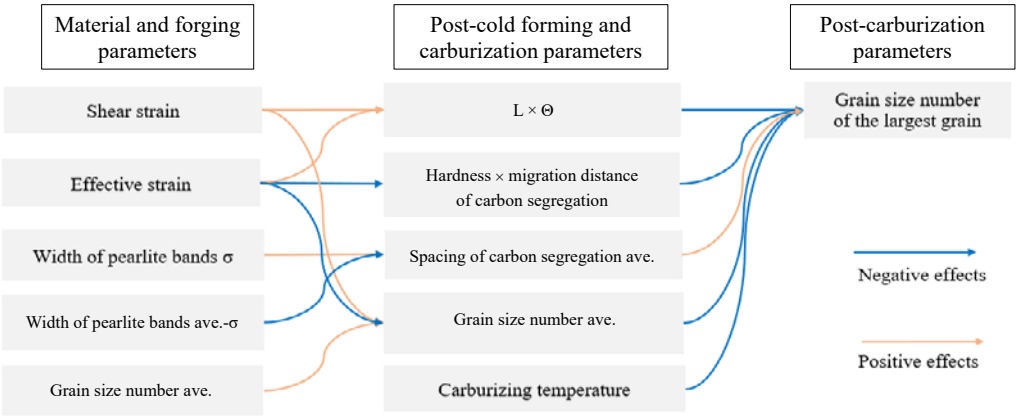


Fig. 5 The DAG in this study

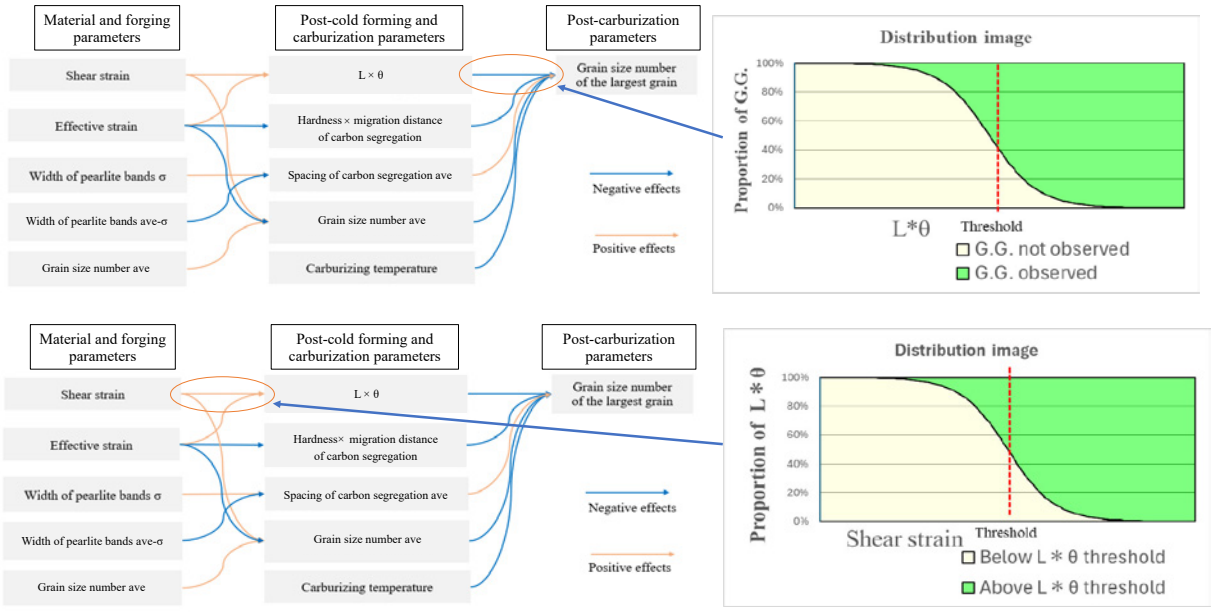


Fig. 6 Setting of threshold values

### 4.4 Construction of Bayesian networks

The results from Sections 4.1 to 4.3 were integrated to construct a Bayesian network. In a Bayesian network, when an explanatory variable (e.g., one of the material parameters) is varied, its effect is propagated through the network, and the probability distribution of the other related explanatory variables (post-cold-forming parameters) is updated. This update is ultimately reflected in the predicted probability of the objective variable (presence or absence of G.G. occurrence).

Using this characteristic, the material and process parameters can be varied to indicate the range of conditions under which G.G. may occur.

## 5. Method to validate the prediction and its results

To verify the accuracy of the created model, leave-one-out cross-validation was conducted using all combinations (108 combinations) (Table 2). First, the AI was trained using the data for all combinations, except for one. Subsequently, the actual data for the material and process parameters of the excluded combination were input into the trained prediction model to predict the occurrence of G.G. The results were verified to determine if they aligned with the actual data.

The verification revealed that the prediction results of G.G. occurrence with material and process parameters as input agreed with the actual data for 79 combinations (Table 3).

Table 2 Leave-one-out cross-validation method

| | Validation pattern | | | | | | |
|---|---|---|---|---|---|---|---|
| | 1 | 2 | 3 | 4 | ・・・ | 107 | 108 |
| Data No. 1 | × | ○ | ○ | ○ | ・・・ | ○ | ○ |
| No. 2 | ○ | ○ | ○ | ○ | ・・・ | ○ | ○ |
| No. 3 | ○ | ○ | ○ | ○ | ・・・ | ○ | ○ |
| No. 4 | ○ | ○ | ○ | ○ | ・・・ | ○ | ○ |
| No. 107 | ○ | ○ | ○ | ○ | ・・・ | ○ | ○ |
| No. 108 | ○ | ○ | ○ | ○ | ・・・ | ○ | ○ |

○ : Training data

× : Validation data

Table 3 Prediction results of G.G.

| | Result |
|---|---|
| Occurrence | 96% (22/23) |
| Non-occurrence | 67% (57/85) |
| Total | 73% (79/108) |

## 6. Improving the accuracy of the prediction model

Although the prediction results were highly accurate in terms of predicting complex phenomena, the accuracy was 67% for G.G. non-occurrence in actual component manufacturing, which is lower than expected (Table 3). To improve the accuracy of the conditions required to avoid G.G. in component manufacturing, we reviewed the decision criteria within the range of conditions appropriate for actual manufacturing. As a result, prediction accuracy improved to 88%, as shown in Fig. 7. Consequently, the manufacturing conditions that do not cause G.G. can be predicted with high accuracy.

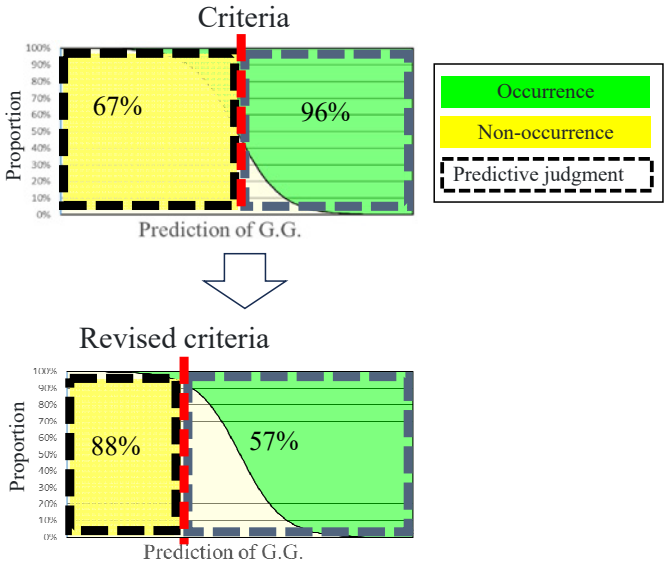


Fig. 7 Modified decision criteria improved non-G.G. precision to 88%

## 7. Conclusion

A technology was developed to optimize manufacturing processes using AI, to predict abnormal grain growth (G.G.) in steel crystals, which has been difficult to predict in previous studies. The following findings were obtained:

[1] The occurrence of G.G. can be predicted by constructing a Bayesian network that considers the causal relationships among the parameters.

[2] As a result of [1], the manufacturing conditions that do not cause G.G. were predicted with an accuracy of as high as 88%.

## 8. References

(1) Akira Mizuno, Go Kato, Makoto Maeda, Takumi Yoshida, Tsubasa Yamashita, Shuhei Kojima, Junya Inoue: Prediction of Abnormal Grain Growth in Carburized Components using Bayesian Networks, Proceedings of the 2025 Spring Meeting, the Society of Automotive Engineers of Japan, 2025, pp. 1–4, reprinted with permission.

(2) Kazumasa Tsutsui, et al.: Current Trends on Deep Learning Techniques Applied in Iron and Steel Making Field: A Review, Iron and Steel, Vol. 109, No. 6, pp. 464–489 (2023).

(3) Hidenori Yoshimura, et al.: Mechanism of Austenite Grain Coarsening in Case Hardening Steel during Carburizing, JFE Technical Journal, No. 23, pp. 30–35 (2009).

(4) Yoshiaki Masuko: On austenite grain size and mechanical properties of steel, Materials Testing, Vol. 6, No. 46, pp. 446–452 (1957).

(5) Noriki Fujita: Plastic Deformation and Texture Simulation in Steels Based on Computational Materials Science, CAMP-ISIJ, Vol. 37, pp. 387–389 (2024).

(6) Hisaki Ikebata: Polymer Informatics Using PoLyInfo, Chemical Information and Computation Science Journal, Vol. 37, No. 4, pp. 94–98 (2019).

(7) Hui Wang, et al.: An integrated approach for numerically predicting the failure of resistance spot welds, Science and Technology of Welding and Joining, 27, pp. 229–237 (2022).

■ Authors ■

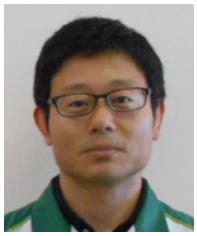
Yasuo ITOU


Gou KATOU


Makoto MAEDA


Takumi YOSHIDA


Tsubasa YAMASHITA


Shuhei KOJIMA


Junya INOUE

# Improving Efficiency in e-Axle System Development through the Integration of MBSE, MBD, and Generative AI

Masaru KATSUKI* Kazunori KAWASHIMA* Takuro KAWASUMI*
Shota SATO** Junji KASHITANI***

## Abstract

To improve the efficiency of e-Axle development, we digitized document-centered systems engineering and integrated it with generative AI. For the digitization, we implemented a meta-structure, introduced mechanisms to reduce the ambiguity in tool dependency, and streamlined the structure. For the AI integration, we compared vector retrieval-augmented generation (RAG) and graph RAG and showed that graph RAG, which is strong in relationship tracking, is effective for information extraction with high accuracy as well as for designers' verification of AI responses by visualizing the basis for the responses.[1]

## 1. Introduction

With the rapid spread of electric vehicles in recent years, improving the quality and efficiency of systems development for electric axles (e-Axles), including the management and effective utilization of heat, has become an important issue.

In the conventional design process, information management based on Requirements, Functions, Logical, Physical (RFLP) is implemented by introducing the concept of systems engineering (SE).[2] However, as shown in Fig. 1, a significant amount of SE information is managed as a large number of documents that are divided by hierarchy and corresponding systems. As such, designers must search for the necessary information by going back and forth between documents at different hierarchical levels. An example of this problem is that it is extremely time consuming to determine how a change in a certain design value affects the entire system.

In recent years, significant progress has been made in generative AI in the form of large language models (LLMs). In the field of SE, an approach for training generative AI to learn the system requirements of model-based SE (MBSE) has been reported.[3]

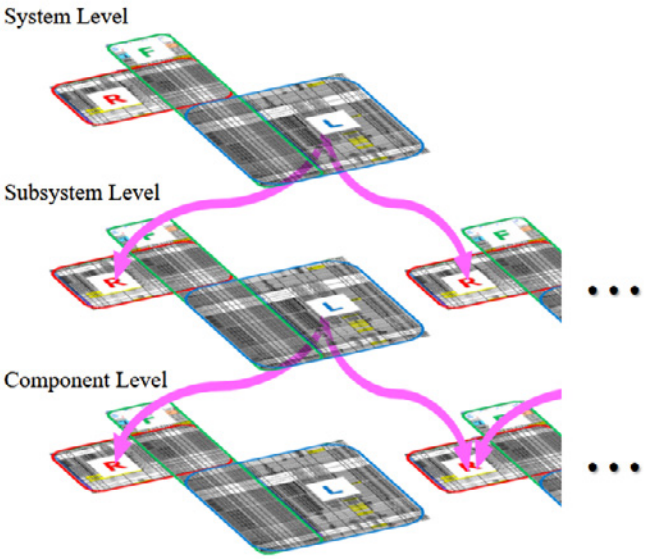


Fig. 1 SE Management form

*Innovative Technology Development Department **Lightblue K.K. ***Panasonic System Design Co., Ltd.

This study applied MBSE to RFLP across multiple levels. As shown in Fig. 2, using MBSE as a foundation, this study aimed to improve the efficiency of information extraction by integrating it with generative AI and to increase the efficiency of analysis preparation and result sharing in conjunction with model-based development (MBD), thereby increasing the development speed and competitiveness.

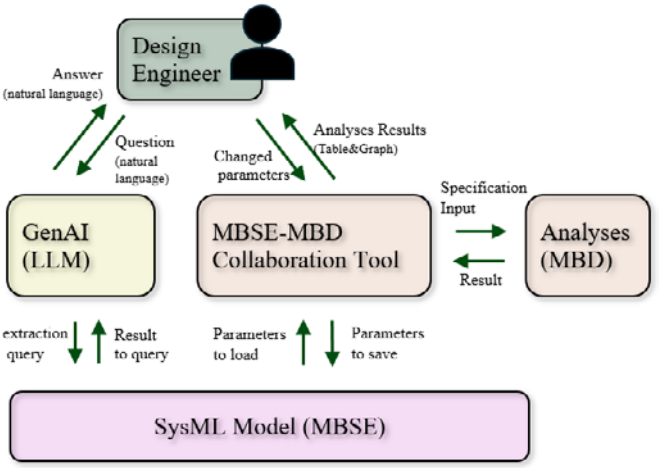


Fig. 2 Overview of this research initiative

## 2. Implementation of MBSE

MBSE is an SE approach centered on digital models, which are modeled using systems modeling language (SysML). MBSE is the foundation of this research and, when building an MBSE model based on SE information in the conventional document forms, there is the concern that if the structure of the MBSE model is not consistent owing to the degree of freedom of SysML tools or individual differences among designers, the answers obtained will be inaccurate even when integrated with generative AI. Therefore, we define a meta-structure as a set of rules that ensure uniformity in the structure of MBSE models and propose an implementation method that enables model construction according to this meta-structure. The meta-structure is based on the hierarchical structure shown in Fig. 3. The structure was constructed with the upper P and lower R as contact points between the hierarchies, considering that RFLP is managed at each hierarchy level according to the operation of a conventional SE management format with reference to public information.[4]

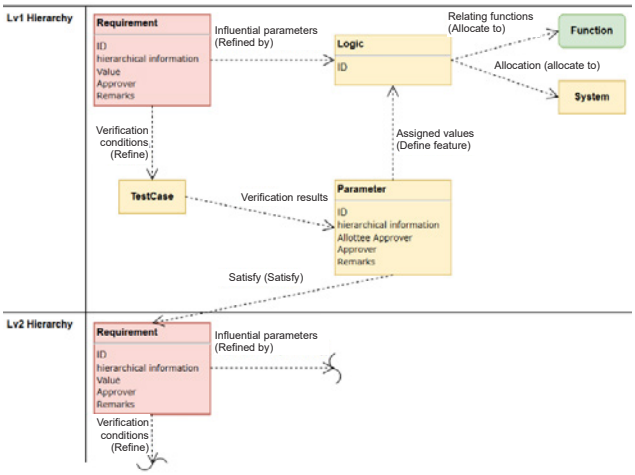


Fig. 3 MBSE meta-structure

The implementation method for the model with the meta-structure consists of a framework and validation rules.

- Framework: A process structure to form the structure of the MBSE model by automatically defining the relationships among elements in accordance with the meta-structure upon inputting information in order into the familiar charts prepared in advance. Figure 4 shows an example.
- Validation rules: A process mechanism to check the relationship between each element, and detect and notify of any omissions or errors. Table 1 presents an example.

These implementation methods enable the construction of a coherent MBSE model that serves as the basis for efficiency improvements.

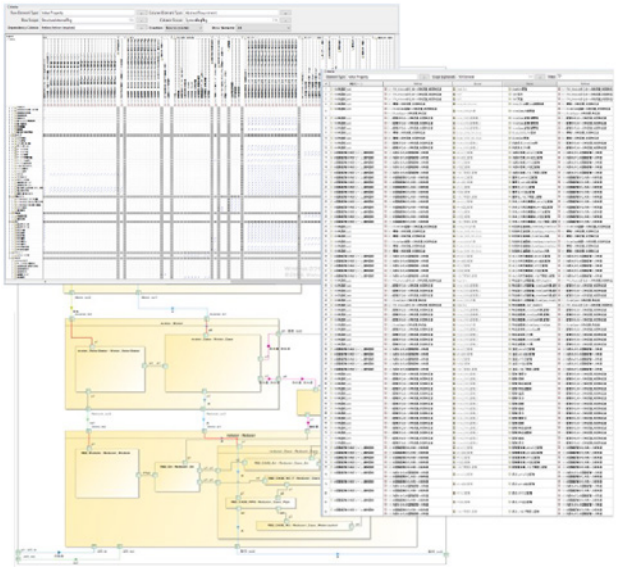

Fig. 4 Example of MBSE modeling framework

Table 1 Example of MBSE validation rules

| # | Restraining factors | Validation rule |
|---|---|---|
| 1 | Function | There must be no factors in refining the Functions |
| 2 | Requirement | The destination of the refined Requirements is TestCase only |
| 3 | Requirement | Requirement is refined only by Logic and TestCase |
| 4 | Requirement | Requirement must be satisfied by Logic |
| 5 | Requirement | Requirement must be refined by Logic |
| 6 | TestCase | The destination of the refined TestCase is Requirements only |
| 7 | TestCase | Only Requirement and TestCase must refine TestCase |

## 3. Design support methods using a combination of MBSE and generative AI

To improve the efficiency of information extraction from the relationships between documents at different hierarchical levels, the MBSE model described in the previous section was integrated with generative AI. The following two approaches were tested as the integration methods based on information retrieval.

The first method is known as vector retrieval-augmented generation (RAG). In this method, the MBSE model is segmented into appropriate units and each segment is converted into a numerical vector. The designer's query is similarly converted into a vector and highly relevant information is retrieved based on the similarity between the two, up to the top-Nth information. This system is highly versatile because it can retrieve information based on similarities in context and meaning.

The second method is named graph RAG, in which the search targets are expressed as a knowledge graph. This method represents information entities as nodes and relationships among information as edges. The retrieval accuracy is expected to improve in terms of capturing the relationships between information and comprehensiveness compared with vector RAG, which is based only on similarity. In the MBSE model constructed in this study, we transformed graph RAG into a knowledge graph such that the meta-structure was maintained.

Figure 5 shows the structure of the graph RAG. When a designer asks a question, the generative AI automatically generates a query to obtain the information necessary to answer the question and look up the knowledge graph. After comparing the information obtained from the knowledge graph with the content of the question, the generative AI generates an appropriate response. To improve the query generation accuracy, few-shot learning is performed for each pattern described below, in which the AI is trained using a set of questions and appropriate queries as the training data.

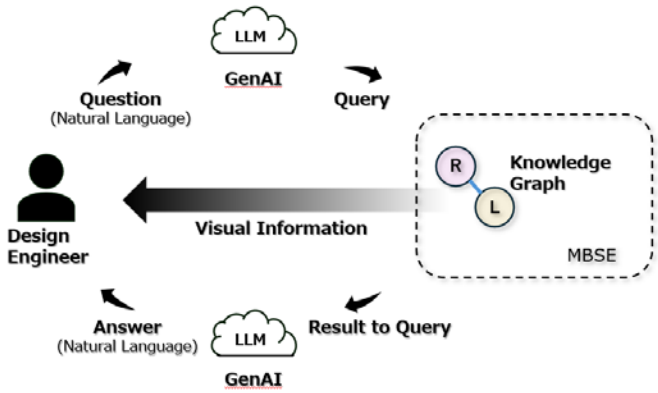


Fig. 5 Configuration of knowledge graph RAG

To verify the effectiveness of the two design support methods, we prepared a set of questions that simulated an actual design situation (Table 2), and evaluated the accuracy of the responses to each of the four question patterns (A to D). The results are shown in Fig. 6. Using the vector RAG, correct answers were obtained only for Pattern A, but not for Patterns B, C, and D. In contrast, Graph RAG provided a high percentage of correct responses for all patterns (A, B, C, and D).

Table 2 Question pattern classification for generative AI responses

| Pattern | Classification | Example questions |
|---|---|---|
| A | Extraction of information of specific elements | What is the required value of the motor coil temperature [°C]? |
| B | Extraction of relationships within specific subsystems and components | Extract all elements that determine the A dimension of the XX part |
| C | Extraction of relationships across hierarchies | If the dimension A of part XX is changed, what are the dimensions of the other parts that are affected by the change? |
| D | Extraction of high-impact factors | What are the top 3 most influential factors in the e-Axle unit? |

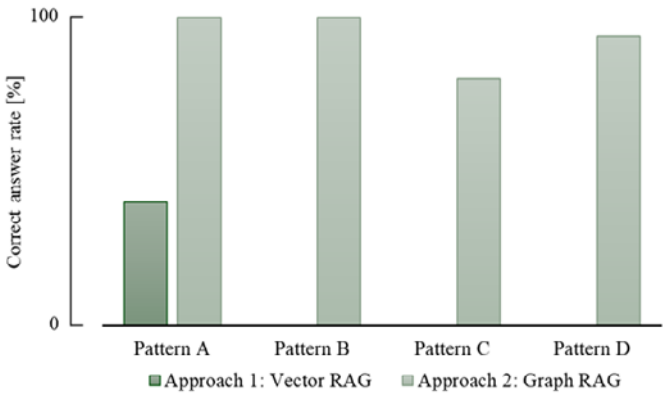


Fig. 6 Generative AI response accuracy evaluation results

In particular, it was confirmed that design parameters can be easily extracted in terms of the size of the influence, which is difficult to grasp solely through visual inspection of the model, such as pattern D. Figure 7 shows an example of actual questions and answers in the graph RAG. In this example, the knowledge graph returns the calculation results for the eigenvector centralities of the nodes.

Question

What are the top 3 most influential factors in the e-axle unit?

Answer

The top 3 most influential factors are listed.
If there are more than one factor with the same level of influence, all of them will be extracted.

1. **Performance (Score: aaa)
1. **Performance (Score: aaa)
2. **Frequency (Score: bbb)
3. **Performance (Score: ccc)
3. **Conditions (Score: ccc)

These are the most influential factors.

Fig. 7 Practical example of a question and answer in the graph RAG approach

It was also confirmed that the designer can verify the results of the responses and visually understand the complex dependencies by referring directly to the knowledge graph in conjunction with the results of the generative AI responses. Figure 8 shows an example of the visualization of the information extracted from the entire knowledge graph and referenced in the answers.

The results confirm that, based on the MBSE model with the meta-structure as an important factor, the graph RAG method can be used to extract information accurately and efficiently.

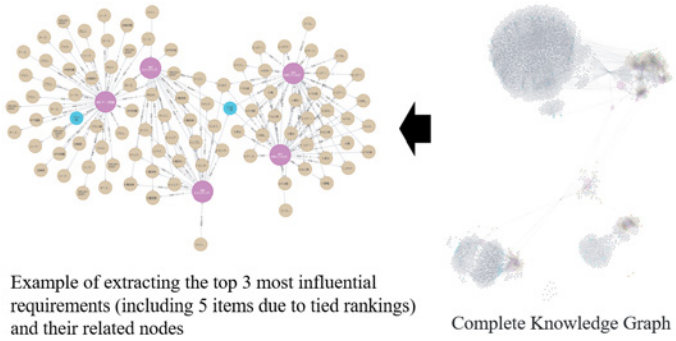


Fig. 8 Example visualization of the queried knowledge graph

## 4. Implementation of an MBSE model for increased analytical efficiency

The dispersion of information shown in Fig. 1 can affect the analysis, and a problem arises whereby significant time and effort are required to verify the latest information, input analysis data, and organize the results. In contrast, the implementation of a coherently structured MBSE model enables seamless connection via the MBSE-MBD collaboration tool. This collaboration reduces the designer's workload and improves efficiency.

The effectiveness of this MBSE-MBD collaboration was confirmed by applying the integration to a small-scale design process. Figure 9 shows the flow of the application process used to determine the specifications in a thermal management analysis.

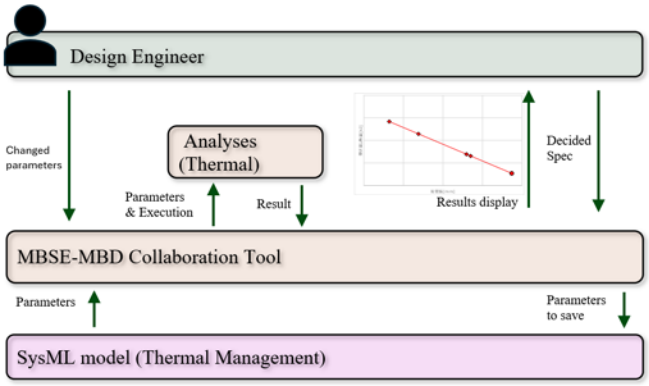


Fig. 9 Example of applying MBSE-MBD collaboration

It was confirmed that the MBSE-MBD collaboration enables the designer to automate the tasks of setting input conditions and organizing results, thereby reducing the time spent on analysis work by 30% (Fig. 10).

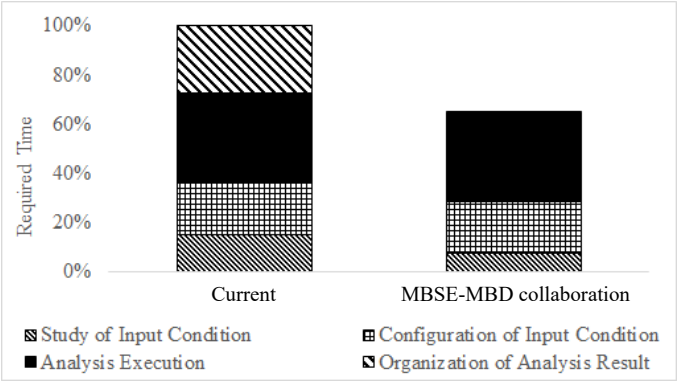


Fig. 10 Efficiency of MBSE-MBD collaboration

## 5. Summary

In this study, SE information in document form was reconstructed as an MBSE model, which was used to improve the efficiency of information extraction through analysis (MBD) and generative AI. In particular, it was demonstrated that graph RAG, which uses knowledge graphs, is superior to vector RAG in its integration with generative AI. It was confirmed that graph RAG enables information extraction with high accuracy in a manner that reflects the model structure. It was also shown that the analysis work itself can be performed efficiently by linking with MBD through the construction of an MBSE model.

In the future, we aim to improve the accuracy of the responses to questions that cannot currently be answered accurately, such as questions with a large number of relationships across hierarchical boundaries. In addition to directly answering the questions of designers, the system will be developed into a more active support tool that complements and expands designers' thinking by providing designers with information on related quality issues and past design knowledge and predicting potential risks. Furthermore, the application scope of generative AI will be expanded to areas that currently need to be handled manually, such as the operation of MBD collaboration tools, to improve the efficiency of the entire design process further.

We will aim to create an environment in which designers can concentrate on more creative work by developing the tool into an AI agent that can understand the designer's intentions, interpret the results by performing parameter selection and optimization analysis autonomously, and propose the next action.

## 6. References

(1) Masaru Katsuki, Kazunori Kawashima, Takuro Kawasumi, Shota Sato, and Junji Kashitani: Improving Efficiency in e-Axle System Development through the Integration of MBSE, MBD, and Generative AI, Proceedings of 2025 JSAE Annual Congress (Spring), Society of Automotive Engineers of Japan Inc., 2025, pp. 1-4, reprinted with permission.

(2) Tsutomu Mochizuki and Hirofumi Michioka: Implementation of systems engineering in transmission development -Efforts to utilize MBSE-, JATCO Technical Review, No. 19, pp. 19-28 (2020).

(3) Braxton VanGundy, Nipa Phojanamongkolkij, Ramana Polavarapu, Barclay Brown, and Joshua Bonner: Requirement Discovery Using Embedded Knowledge Graph with ChatGPT, 34th Annual INCOSE International Symposium, pp. 2011-2027 (2024).

(4) Aistė Aleksandravičienė and Aurelijus Morkevičius: MagicGrid® BOOK OF KNOWLEDGE A Practical Guide to Systems Modeling using MagicGrid from Dassault Systèmes, 2nd edition, Lithuania, Vitae Litera, UAB, 2021.

■ Authors ■


Masaru KATSUKI


Kazunori KAWASHIMA


Takuro KAWASUMI


Junji KASHITANI

# AI-Driven Digitalization for an Automotive Component Manufacturer

Ruowen HE* Chunhui ZHENG* Jianbo HUANG*

## Abstract

In the automotive industry, operational efficiency has been increasing because of digitalization and smart-factory transformation. To maintain competitiveness in this landscape, we developed an AI agent system that links retrieval-augmented generation to large language model. The system was applied to eight business scenarios, including knowledge retrieval and translation.

## 1. Introduction

The automotive industry is making rapid progress in improving operational efficiency through digitization and smart-factory transformation, and it is imperative for our company to apply these technologies in practice. In this study, we introduce our administrative initiatives at JATCO (Guangzhou) Automatic Transmission Ltd. In the area of administration, there are a wide variety of tasks such as knowledge retrieval, information organization, and contract review, and it is necessary to support not only specific tasks but also a wide range of them. In this study, we built a system that can be applied to actual operations by optimizing preprocessing, post-processing, and prompting, based on a method that combines retrieval-augmented generation (RAG) and a large language model (LLM).

### 1.1 Definition of terms

1) LLM [1]

Large language models are pretrained on large amounts of data and can perform a variety of language processing tasks (e.g., translation and analysis).

2) RAG [2]

A technology that retrieves relevant knowledge from external databases (e.g., terminology dictionaries and internal documents) in real time and augments the LLM to improve the accuracy of its responses.

3) Hybrid similarity

A retrieval evaluation index for a RAG system, which indicates the overall literal and semantic matching between the query and documents by calculating the weighted combination of keyword and vector similarities. Values range from 0% to 100%, with higher values indicating better overall matching.

4) Keyword similarity

A retrieval evaluation index for a RAG system that indicates the degree of lexical matching based on keyword overlap between the query and documents. Values range from 0% to 100%, with higher values indicating better lexical matching.

5) Vector similarity

A retrieval evaluation index for a RAG system that indicates the semantic similarity between a query and documents through high-dimensional vector transformation. Values range from 0% to 100%, with higher values indicating better semantic matching.

*Corporate Planning Department

## 2. Methodology and approach

### 2.1 Business analysis and the selection of core technology

In this study, we focused on high-frequency and high-volume work scenarios identified through an internal questionnaire. These include eight core business scenarios (Table 1), such as knowledge retrieval, translation, program coding, and contract review, covering a wide variety of practical cases, from general-purpose to specialized department-specific situations.

As a technical implementation method, RAG was employed as the core search engine responsible for document processing and vector [3] retrieval to provide high-quality knowledge retrieval. At the same time, an LLM was used as the basis for the language model service to provide the system's core functions of understanding language and generating texts.

This system presents and introduces novel processing methods for the pre- and post-processing for RAG and LLM to enhance the effectiveness of the final output in each scenario. As shown in Fig. 1, the overall structure of the system is the integrated flow of knowledge retrieval and language processing by linking RAG and LLM.

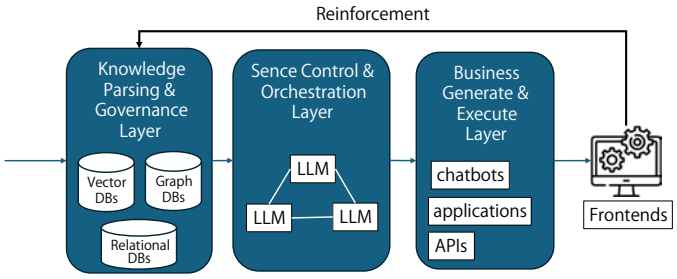


Fig. 1 Configuration of the system

### 2.2 Preprocessing

Preprocessing is a fundamental process that determines the accuracy, stability, and business compatibility of the RAG and LLM-based AI agent system. In the business scenarios targeted by this system, such as knowledge retrieval and translation, the documents to be processed are in a variety of formats, including PDF, Microsoft Word, and Microsoft Excel Note [Note1]. Hence, it is difficult to satisfy all business needs using a single preprocessing step.

In the preprocessing of this system, we used the "common infrastructure + scenario specialization" approach (Fig. 2) and designed preprocessing strategies according to the characteristics of each task. That is, common processes such as document structure analysis and semantic extraction were standardized, while specialized processes were developed by including the strategic conversion of the document format for knowledge retrieval, as well as structuring and reconfiguration of contents to preserve the structural elements of source documents and ensure semantic consistency.

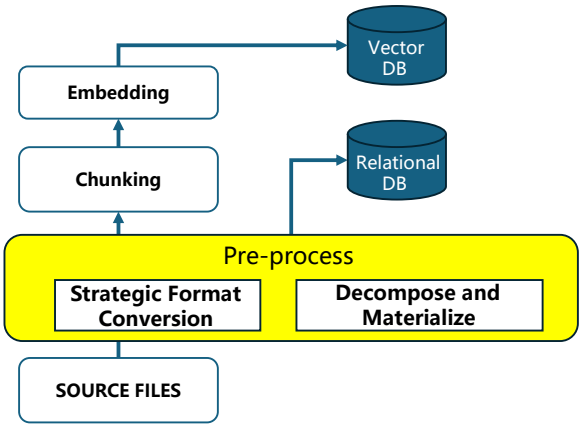


Fig. 2 Preprocess of RAG

Table 1 Matrix of departments and works

| Department | Knowledge retrieval | Information organization | Program coding | Translation and Interpretation | Request and submission for approval | Contract review | Application proxy service | PC kitting |
|---|---|---|---|---|---|---|---|---|
| Production Engineering | R | R | R | I | I | I | I | - |
| Information System | A | A, R | A, R | A, R | R | R | R | A, R |
| Management | R | R | R | I | C | C | A | - |
| Finance | R | R | R | I | I | I | I | - |
| Legal Affairs | R | R | R | I | A | A | I | - |
| Purchasing | R | R | R | I | I | I | I | - |
| Manufacturing | R | R | R | I | I | I | I | - |

RACI: I (Informed)
C (Consulted)
R (Responsible)
A (Accountable)

Note 1: Microsoft Word and Microsoft Excel are registered trademarks of Microsoft Corporation.

### 2.2.1 Strategic format conversion [8]

In a RAG system, the quality of document parsing has a direct impact on search effectiveness. Conventional methods directly parse documents in their original format (particularly Excel files), resulting in serious problems, such as “semantic fragmentation” and “loss of structural information.” The reason is that the division of Excel files relies mainly on mechanical processing based on worksheets and a fixed number of rows, which hinders the understanding of matrix relationships among cells and the semantic linkage of data, resulting in the fragmentation of information and loss of structural linkage. Furthermore, Excel analysis often uses lightweight processing libraries and lacks the multistep processing mechanisms based on layout analysis and semantic understanding, which are widely used in PDF parsing. This makes it difficult to preserve the hierarchical structure of complex tables or logical relationships among data. To build a standardized processing infrastructure, the system first converts various documents into PDF files in a unified manner. PDF files have a fixed layout and stable structure, which are advantageous for preserving the original layout and semantic integrity of the document. Thus, the accuracy of the analysis is significantly improved over the direct processing of complex Excel source files.

### 2.2.2 Structure analysis and reconstruction of contents

Knowledge retrieval and translation are important application scenarios in the digitalization of business operations. Although both share a technical foundation in the layers of document parsing and semantic understanding, the complex tables, graphs, and other structural elements contained in Excel files are format-sensitive and prone to problems, such as broken layout, distorted meaning, and disconnected context, in a generic translation process.

There are two important data processing solutions to this problem.

1) Text elements (e.g., cells, comments, and graph labels) in Excel files do not exist in isolation, but their positions and combined states constitute an important semantic context. Therefore, Excel elements were extracted using an in-house Extractor and stored in a database (Table 2). Note that the structure shown here is a schematic and not the complete table structure of the actual business scenario.

Table 2 Structured tokens of the text

| Idx | File name | Sheet name | Element type | Location | Row | Contents | Result |
|---|---|---|---|---|---|---|---|
| 1 | File 1 | Sheet 1 | Cell | $A$1 | 1 | Test 1 | |
| 2 | File 1 | Sheet 1 | Cell | $A$1 | 2 | Test 2 | |
| 3 | File 1 | Sheet 2 | Shape | Shape name | 2 | Test 1 | |

2) The Extractor has a function that allows customization of extraction patterns and filtering of characters according to the operational scenario. For example, when using LLMs, it is possible to exclude elements that do not need to be translated, such as simple “〇”, “-”, and numbers, to ensure translation accuracy and speed.

### 2.2.3 Prompt engineering

The source text is entered to be batch-translated and a prompt is created.

Example prompt:

1. Input format：{{Idx} 和文原文 };{{Idx} 和文原文 };...（Idx はインデクスの数字）
2. Output format：{{Idx} 中文翻訳 }};{{Idx} 中文翻訳 };...

Example of a text to be translated:

……

{{1} テスト 1};{{2} テスト 2};{{3} テスト 1};

……

Example of an AI response:

……

{{1} 测试 1};{{2} 测试 2};{{3} 测试 1};

……

Note that the prompts shown here are schematic examples based on Table 2, and not actual operational scenarios.

To input the translation from AI responses into the next process, the system first uses a regular expression (e.g., '\{\{(\d+)\}(.*?)\}') [6] to match the fixed structure of "{{Idx}Translated text}". In the initial step, it detects structural breakdowns caused by the LLM's hallucination (e.g., `{{1}测 试1` (lack of closing brackets), `{{A}测试1}` (Idx is not a number), and `{{3}测试3}` (content consistency breakdown)).

Next, "verification of structural breakdowns" is performed based on the results of the regular expression analysis. Specifically, the number and type of detected breakdowns are determined, and if a threshold (e.g., one or more breakdowns) is exceeded, then the LLM is re-directed to "generate responses that comply with the structure" (re-execution design). This avoids the negative effects of structural breakdowns caused by the LLM's hallucination and guarantees the accuracy of the translation extraction.

To solve the problem of terminology mismatch, this study introduced a dynamic terminology reinforcement mechanism in the translation command generation phase (Fig. 3). The system searches the terminology dictionary in real time and embeds the identified terms and their in-house standard translations into the LLM prompts as mandatory constraints, thereby fixing the translation of keywords from the source side and ensuring terminology consistency throughout the whole text.

Optimally structured prompts are embedded in LLM requests to ensure stable outputs in cases such as large translation jobs.

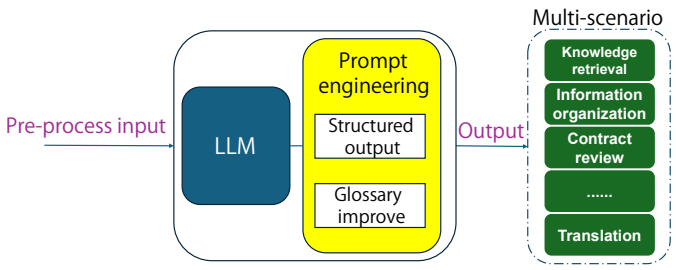


Fig. 3 Prompt engineering

## 2.3 Post-processing

### 2.3.1 Competitive optimal selection of dual LLMs [7]

To address the bias of a single model, this study employed parallel translation using dual LLMs and an automatic optimal-selection mechanism (Fig. 4). After completing the "phase matching" of the translation, the system performs comparison and scoring for each based on multidimensional criteria such as the degree of terminological matching, contextual accuracy, and naturalness of language flow, and automatically selects the best overall translation. This optimal selection mechanism effectively combines the strengths of different models to achieve significant improvement in translation quality.

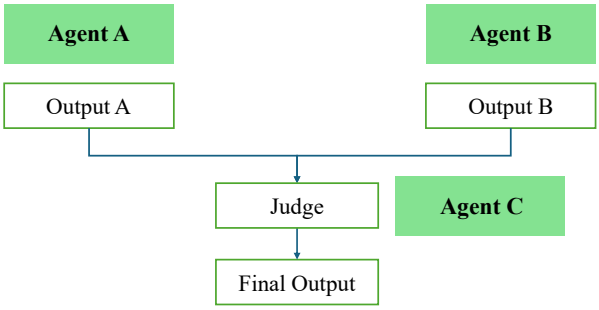


Fig. 4 Optimal selection of dual LLM outputs

### 2.3.2 High-precision image processing

This study also solved the problem of translating images in documents. Common image translation tools or application programming interfaces usually have difficulty preserving the visual layout of the original image. To solve this problem, a refined image processing subprocess was designed. The core steps and technical challenges are described below.

1) Optical character recognition [4], [5] and the structuring of text and coordinates

First, bulk extraction of embedded images in Excel was performed. Then the text content and its bounding box coordinates (A, B, C, and D) are recognized by optical character recognition (OCR). This process converts the image information into structured data containing text and coordinates, then establishes the basis for subsequent high-precision processing (Fig. 5).

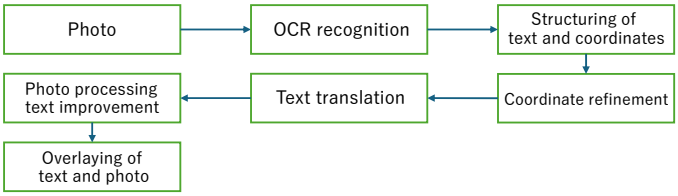


Fig. 5 Use of position information in text OCR

2) High-precision calibration of text coordinates

To address the problem of errors in the coordinate recognition by OCR, an automatic coordinate correction algorithm was designed. The coordinates were refined pixel-by-pixel using a “dual slider” mechanism. In addition, the final coordinates after refinement (A1, B1, C1, and D1) were determined by judging the validity of text recognition (e.g., correctness of character segmentation and reasonableness of blank areas) using the algorithm (Fig. 6).

3) Text translation, rewriting, and image composition

After obtaining the precise coordinates, the system performs LLM translation of the recognized text. Subsequently, based on the calibrated coordinates, the system renders the translated texts in the appropriate font and overlays them on the original image to complete the generation and reconstruction of a high-quality translated image.

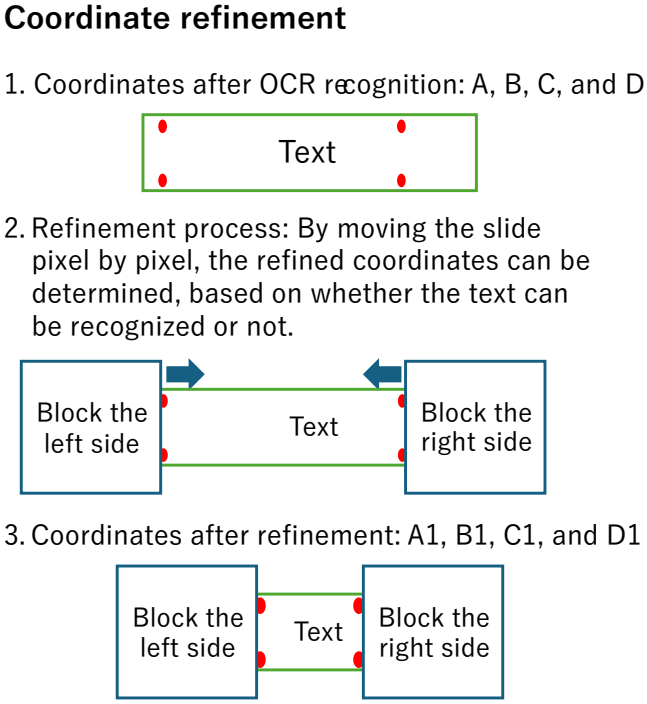


Fig. 6 Refinement of text position

## 3. Result

As discussed in Sections 2.2 and 2.3, the integration of preprocessing and post-processing with the AI agent system of this study (a combination of RAG and LLM) greatly improved the accuracy of the AI’s responses.

### 3.1 Effects of preprocessing

To evaluate the effects of unifying documents formats into PDF in the process of normalizing specific file formats, a comparison experiment was conducted using vector searches (Table 3). The keyword similarity was consistent under the same query because of the same matching content of keywords in the content of the chunks. PDF chunks had higher vector similarity in most cases, demonstrating that their semantic structure was better preserved.

Table 3 Effect of file format conversion

| File format | Average hybrid similarity [%] | Average keyword similarity [%] | Average vector similarity [%] |
|---|---|---|---|
| Excel | 71.86 | 73.95 | 66.98 |
| PDF | 74.8 | 73.95 | 76.78 |

In this experiment, the performances of two representative LLMs (LLM A and LLM B) were compared in standard and terminology-enhanced prompts. The mean values of each group were calculated after multiple repetitions. As shown in Fig. 7, terminology injection improved the terminology usage rate from 32% to 98% in LLM A and from 22% to 86% in LLM B, resulting in a significant average improvement of 65 percentage points.

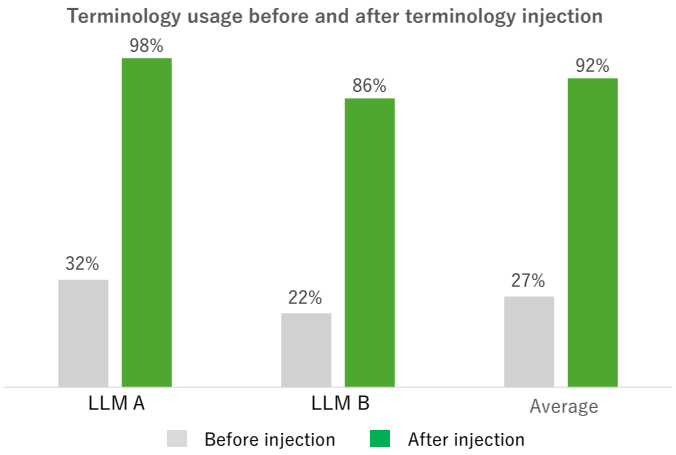


Fig. 7 Terminology injection effect

## 3.2 Effects of post-processing

We performed translation on a dataset using two different LLMs and found differences between the outputs. The average translation accuracy of a single LLM was 96%. However, by introducing an optimal selection mechanism using a third LLM to determine the translation differences between the two LLMs, the overall translation accuracy increased to 97%. This result suggests that it is possible to improve translation accuracy through a cooperative mechanism using multiple LLMs.

For high-precision image processing, the coordinate refining process significantly improved the consistency of the translation from Chinese to Japanese, as shown in Fig. 8.


Fig. 8 Coordinate precision effect

Finally, through the translation of a large volume of technical documents used in this development, an independent accuracy-oriented technical route was designed, and a mixed strategy of “parallel processing with dual LLMs, semantic enhancement (RAG), structured control, and optimal selection of results” was adopted. The overall test results showed that the consistency in the translation of internal terminology and overall quality of the translation were significantly improved, and the structural elements were effectively preserved. Compared with the previous business process, the total number of labor hours required for translation was also significantly reduced. In particular, the translation of texts within images has effectively eliminated traditional issues such as coordinate misalignment, enabling the stable provision of high-quality translation necessary for accurate communication and sharing of technical information.

By applying the above methods, the system achieved both “accuracy improvement” and “efficiency improvement” in a wide range of administrative tasks at an automotive parts manufacturer.

## 4. Discussion

In this initiative for improved system efficiency, the results were manifested by the cooperative mechanism between RAG and LLM. Specifically, RAG searched and reinforced terminology and in-house knowledge from external databases in real time, which suppressed the LLMs' hallucination and improved the consistency of terminology in translation and the accuracy of contract reviews. At the same time, in knowledge retrieval operations, high-quality knowledge recall by RAG resulted in significant time savings compared with conventional manual retrieval. Thus, knowledge-retrieval capability is the foundation for both business compatibility and processing accuracy of the AI system; it is an essential element for the practical application of AI collaboration and its utilization.

Accurate semantic chunking is a core factor in improving the retrieval accuracy of RAG. Structured data-preprocessing approaches-such as extracting content contained within shape frames or image elements during Excel translation-offer new ideas for semantic chunking in other file formats.

## 5. Conclusion

The results of this study demonstrated that the cooperative model of knowledge retrieval capability by RAG and language processing capability by LLM is highly adaptable and effective in improving the efficiency of a wide variety of administrative tasks in the automotive parts manufacturing industry. This model provided a solution for both automation and quality assurance of complex document processing, providing a new perspective on the practical application of AI technology in the smart-factory transformation of the automotive industry.

## 6. Summary

In this study, an AI agent system that links RAG and LLM was used to digitalize tasks and reduce labor hours in administrative areas. The use of AI technology in our company is not limited to the administrative department, but is also applied to the production floor, where image processing and deep learning are used to automate inspections of machining processes.

After one year of operation of the AI agent system, it was found that the total labor hours saved in eight work scenarios reached 1,837 hours per year, including translation and interpretation (722 h) and knowledge retrieval (381 h), as shown in Table 4.

Table 4 Labor hour reduction effect

| Core business scenarios | Reduction in man-hours (h) |
|---|---|
| Translation and interpretation | 722 |
| Knowledge retrieval | 381 |
| Application proxy service/PC kitting | 243 |
| Contract review/request and submission for approval | 240 |
| Program coding | 231 |
| Information organization | 20 |

The following four challenges need to be addressed in the future.

1) Further application of the pre- and post-processing architecture of this study should be considered for wider business scenarios.
2) Output stability and processing speed of each module should be improved further.
3) The architecture and implementation strategy should be adjusted from time to time in keeping with the development of LLM technology.
4) Aimed at advanced applications, role-type agents should be developed, such as assistants for office work execution, meeting moderators, educational lecturers, predictive maintenance assistants for facilities, and assistants for designing parts.

## 7. References

[1] Alammar, J. & Grootendorst, M. (2024). Hands-On Large Language Models. O'Reilly Media. (Official code repository: https://gitcode.com/GitHub_Trending/ha/Hands-On-Large-Language-Models).

[2] Lewis, P., Perez, E., Piktus, A., Petroni, F., Karpukhin, V., Goyal, N., Küttler, H., Lewis, M., Yih, W. T., Rocktäschel, T., Riedel, S., & Kiela, D. (2020). Retrieval-Augmented Generation for Knowledge-Intensive NLP Tasks. Advances in Neural Information Processing Systems, 33 (NeurIPS 2020). arXiv Preprint arXiv:2005.11401. https://doi.org/10.48550/arXiv.2005.11401.

[3] Johnson, J., Douze, M., & Jégou, H. (2019). FAISS: A Library for Efficient Similarity Search and Clustering of Dense Vectors. Research Facebook, arXiv Preprint arXiv:1702.08734. https://doi.org/10.48550/arXiv.1702.08734.

[4] Cheng Cui, Ting Sun, Manhui Lin, et al. PaddleOCR 3.0 Technical Report [Online]. 2025. arXiv:2507.05595 [cs.CV]. https://arxiv.org/abs/2507.05595.

[5] Cheng Cui, Ting Sun, Suyin Liang, et al. PaddleOCR-VL: Boosting Multilingual Document Parsing via a 0.9B Ultra-Compact Vision-Language Model [Online]. 2025. arXiv:2510.14528 [cs.CV]. https://arxiv.org/abs/2510.14528.

[6] Jeffrey E. F. Friedl: Mastering Regular Expressions, 3rd Ed., Sebastopol, CA, O'Reilly Media, Inc., 2006, 515 pages. ISBN: 0-596-52812-4

[7] Zhang, Y., Li, J., & Chen, W. (2023). JudgeLLM: Evaluating and Selecting LLM Outputs via a Specialized Judge Model. In Proceedings of the 2023 Conference on Empirical Methods in Natural Language Processing (EMNLP), pages 8924–8938, Singapore. Association for Computational Linguistics. https://doi.org/10.18653/v1/2023.emnlp-main.521

[8] Zixuan Ke, Yucheng Wang, Yichao Zhou, Jia Li, Yutao Zhu, Yujiu Yang, Yi Liu, Ninghao Liu, Haiyun Jiang, Wayne Xin Zhao, & Zhicheng Dou. (2023). A Survey on Table Understanding in Natural Language Processing. arXiv Preprint arXiv:2305.13095. https://doi.org/10.48550/arXiv.2305.13095

■ Authors ■


Ruowen He


Chunhui Zheng


Jianbo Huang

# Introducing the Jatco CVT-S (JF021E) for the Nissan ROOX, Mitsubishi Delica Mini and Mitsubishi eK Space

Jatco CVT-S was installed into ROOX, Delica Mini, and eK Space, which were released by Nissan and Mitsubishi Motors in October 2025.

Pump noise was reduced by optimizing the design of the oil pump. Weight reduction was achieved with fewer ribs in the transmission case and side covers added as noise countermeasure. Furthermore, the number of pinions on the carrier was reduced from four to three, which is considered difficult to achieve in continuously variable transmission (CVT) due to noise issues in the planetary gear. This successfully reduced the cost, which contributed to improved profitability. In terms of control, the gearshift program was optimized for the characteristics of the new engine specifications, thereby achieving smooth revving in response to the acceleration pedal, making acceleration feel more natural, which has received high praise from customers.

Moreover, five driving modes (POWER, ECO, NORMAL, GRAVEL, and SNOW) were introduced to Delica Mini, which has contributed to improved product appeal.

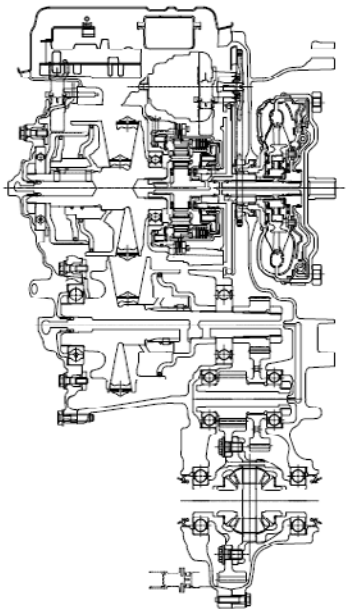

Fig. 1 Main cross-sectional view

Table 1 Specifications of JF021E

| | |
|---|---|
| Torque capacity | 100 Nm |
| Torque converter size | 185 mm |
| Pulley ratios | 2.411–0.404 |
| Auxiliary transmission gear ratios | Fwd 1.000 |
| | Rev 1.000 |
| Ratio coverage | 6.0 |
| Final gear ratio | 7.319 |
| Selector position | P, R, N, D, L |
| Overall length | 356 mm |
| Weight (wet) | 60.6 kg |

ROOX

Delica Mini

eK Space

# Introducing the Jatco CVT-XS (JF023E) for the Nissan Sentra

Jatco CVT-XS (JF023E) was installed into the new Sentra, which was released in North America by Nissan Motor in 2025.

The CVT-XS maximizes the performance of the new Sentra by combining a large ratio coverage with an optimal gear ratio.

CVT-XS features high control performance with a multiplate lockup and a 3-way linear solenoid, thereby offering superior dynamic driving performance and a natural and smooth feeling of acceleration.

The driving performance enabled by JATCO's control technology has further enhanced the attractiveness of the vehicles equipped with CVT-XS, receiving high praise of the customers in the North American market.

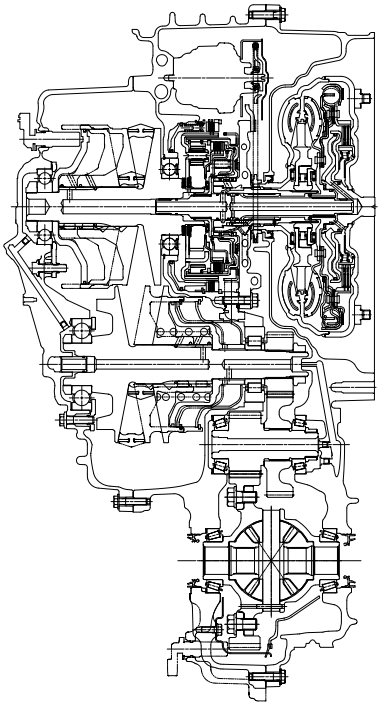

Fig. 1 Main cross-sectional view

Table 1 Specifications of JF023E

| | |
|---|---|
| Torque capacity | 280 Nm |
| Torque converter size | 230 mm |
| Pulley ratios | 2.805–0.357 |
| Ratio coverage | 7.9 |
| Reverse gear ratio | 0.745 |
| Final gear ratio | 5.034 |
| Selector positions | P, R, N, D, B |
| Overall length | 379.9 mm |
| Weight (wet) | 94.6 kg |

Sentra

# Introducing the Jatco CVT8 (JF016E) for the Mitsubishi DESTINATOR

Jatco CVT8 (JF016E) was installed into the new SUV "DESTINATOR" that Mitsubishi Motors started selling in Indonesia in July 2025.

JF016E uses a torque converter and a differential that are optimized for the vehicle and a 1.5 L turbo engine. The gearshift control and adaptation technologies have been refined to provide a high-quality smooth ride in calm driving situations, such as in-city traffic or cruising on expressways, with responsive powerful acceleration when depressing the accelerator pedal during uphill driving or overtaking on expressways.

Jatco CVT8 supports drive modes*, and the driving force has been optimized according to road conditions, contributing to superior driving performance even in two-wheel drive (2WD).

* Five modes can be selected according to road surface conditions.

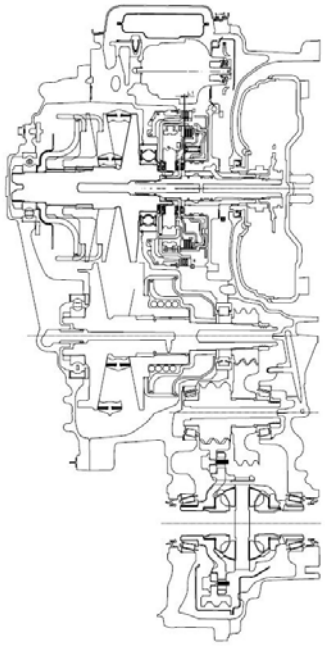

Fig. 1 Main cross-sectional view

Table 1 Specifications of JF016E

| | |
|---|---|
| Torque capacity | 250 Nm |
| Torque converter size | 236 mm |
| Pulley ratios | 2.631–0.378 |
| Ratio coverage | 7.0 |
| Reverse gear ratio | 0.745 |
| Final gear ratio | 6.386 |
| Selector positions | P, R, N, D, L + Ds - SW |
| Overall length | 372.2 mm |
| Weight (wet) | 93.2 kg |

DESTINATOR

# Introducing the “Lifmy” Wheelchair with Transfer Mechanism

Lifmy is a wheelchair with a transfer mechanism developed with the aim of reducing caregiver burden and supporting user independence. It features a scientifically designed lift mechanism that aims to assist users safely and reliably during daily transfers—from bed to wheelchair and from wheelchair to toilet—thus helping with delicate care tasks. By enabling users to utilize their own physical function to stand and move, it seeks to ease both the physical and mental load on caregivers. The stable seat structure is designed to allow users to move comfortably while seated, with the goal of minimizing the risk of falls. Combining JATCO’s automotive technology and quality control, Lifmy strives to contribute to a society where everyone can live actively and with dignity.

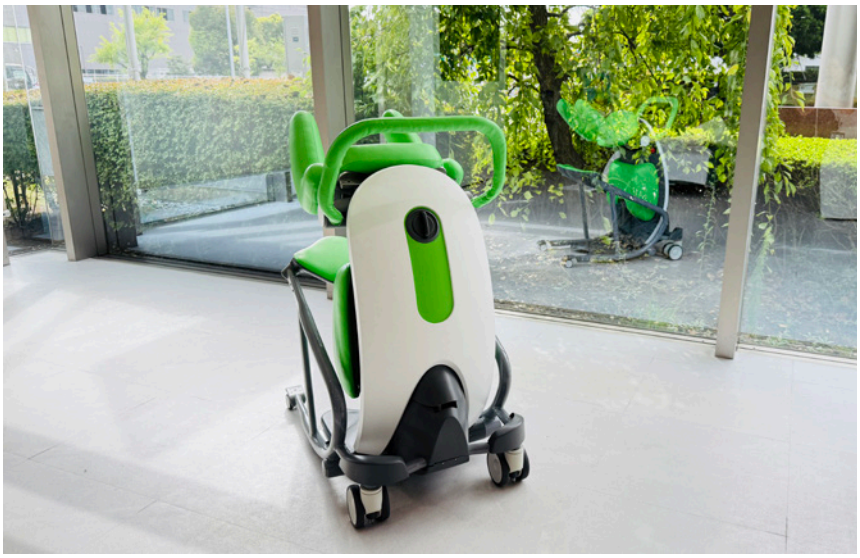

Lifmy

# Patent

This patent relates to an e-Axle mounted on a new type of BEV, as introduced in this technical report.

## 1. POWER TRANSMISSION DEVICE

(Fig. 1)

Application Number :2024-540304
Application Date :28.6.2023
Patent Number :7713111
Registration Date :15.7,2025
Title :POWER TRANSMISSION DEVICE
Inventors :Akira TSUCHIDA

【SUMMARY OF THE INVENTION】

[Problem] The air breather chamber and the oil catch tank can restrict the arrangement of shafts in a power transmission device. This restriction may force shafts that do not necessarily need to be immersed in the oil reservoir to be submerged, potentially leading to increased stirring resistance.

[Solution] According to the present invention, an air breather chamber 10b is provided above and near the third shaft 23. An oil catch tank 10c, which reserves the oil raked up by the gear portion of the third shaft 23, is positioned above and near the first shaft 21. Furthermore, an oil guide 10d, located above the second shaft 22, introduces the oil raked up by the gear portion into the oil catch tank 10c. Crucially, the second shaft 22 is set at a position higher than the axes A1, A3 of both the first and third shafts 21, 23, and is disposed outside the oil reservoir within the case.

As a result, the stirring resistance of a shaft can be reduced as compared with a case in which the second shaft is immersed in the oil reservoir, and the stirring resistance of the shaft in the oil reservoir can be improved.

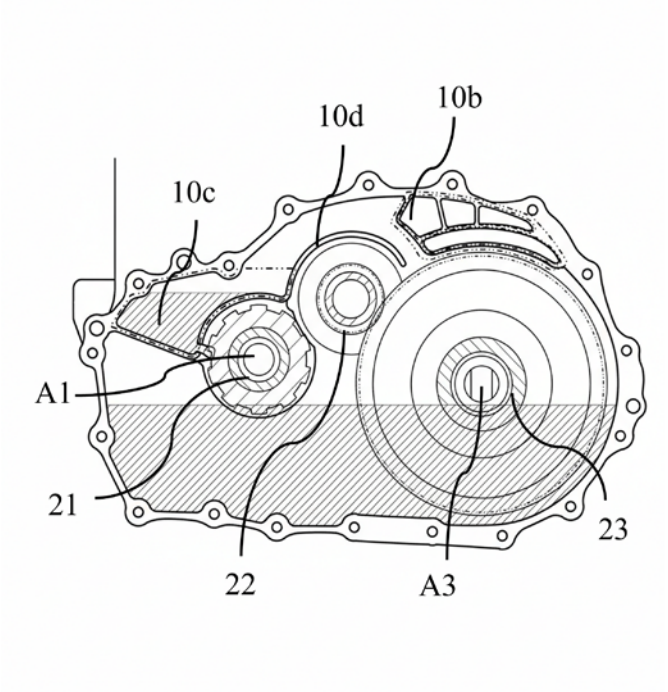


Fig. 1

This patent relates to an e-Axle mounted on a new type of BEV, as introduced in this technical report.

## 2. ROTATING ELECTRIC MACHINE

(Fig. 2)

Application Number :2023-536275
Application Date :20.7,2021
Patent Number :7580609
Registration Date :31.10,2024
Title :ROTATING ELECTRIC MACHINE
Inventors :Yojiro MOCHIZUKI,
Yusuke SUZUKI,
Kazuki EGUCHI,
Tatsuya UCHIDA,
Yiwei ZHAO,
Fumio HONDA

【SUMMARY OF THE INVENTION】

[Problem] In conventional rotating electric machines, if the end portion of the inner housing is not properly centered during press-fitting, the inner housing may be press-fitted into the outer housing in a tilted state, potentially leading to coolant leakage from the sealing portion.

[Solution] According to the present invention, when the inner housing 3 is inserted into the outer housing 4, at the point when the first sealing member 6a contacts the first cylindrical surface and the second sealing member 6b contacts the second cylindrical surface, an axial gap C is formed between the end portion of the inner housing and the third cylindrical surface 43. This configuration ensures that the first sealing member contacts the first cylindrical surface or the second sealing member contacts the second cylindrical surface before the end portion of the inner housing contacts the third cylindrical surface. This configuration enables the inner housing to be centered prior to its press-fitting. Consequently, during assembly of the inner and outer housings, the end portion of the inner housing can be press-fitted without the inner housing tilting relative to the outer housing.

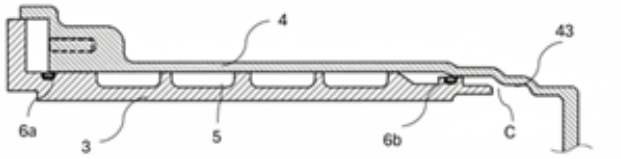


Fig. 2

ジヤトコ テクニカル レビュー No.25

JATCO Technical Review No.25





発行　2026年3月
発行所　ジヤトコ株式会社
イノベーション技術開発部
〒417-8585
静岡県富士市今泉700-1
TEL: 0545-51-0047（代）
FAX: 0545-51-5976
編集　有限会社 BLUE CODE
東京都世田谷区大蔵6-14-14

March 2026
Distributor　Inovative Technology Development Department
JATCO Ltd
700-1 Imaizumi, Fuji City, Shizuoka
417-8585, Japan

**JATCO Ltd**

700-1, Imaizumi, Fuji City, Shizuoka 417-8585, Japan
TEL: +81-545-51-0047  FAX: +81-545-51-5976

**www.jatco.co.jp/english**